A General Track Fit based on Triplets

A. Schöning[a]

[a] *Physics Institute, Heidelberg University, Im Neuenheimer Feld 226, 69120 Heidelberg, Germany*

Abstract

This paper presents a general three-dimensional track fit based on hit triplets. The general track fit considers spatial hit and multiple Coulomb scattering uncertainties, and can also be extended to include energy losses. Input to the fit are detector-specific triplet parameters, which contain information about the triplet geometry (hit positions), the radiation length of the material and the magnetic field. Since the solution is given by an analytical closed-form, it is possible to use the same fitting code for all kind of tracking detectors.

Fitting formulas are given for the global track fit as well as for the local hit triplets. The latter allows filtering out triplets with poor fit quality at an early stage of track reconstruction. The construction and fit of local triplets is fully parallelisable, enabling accelerated computation with parallel hardware architectures. Formulas for the detector-specific triplet parameters are derived for the two most commonly used field configuration for tracking detectors, namely a uniform solenoidal field and gap spectrometer dipole. An algorithm to calculate the triplet parameters for an arbitrary magnetic field configuration is presented too.

This paper also includes a discussion of inherent track fit biases. Furthermore, a new method is proposed to accelerate track fitting by classifying tracking regimes and using optimal fit formulas.

Keywords: tracking, track fit, track fit bias, hit triplet, multiple scattering, fit quality, software alignment, spectrometer, energy loss, tracking regimes

1. Introduction

In nuclear and particle physics experiments, the precise determination of the track parameters for measuring charged particles is crucial. Therefore an accurate tracking model is required that takes into account all error sources of the measurement, the most relevant being hit position errors, multiple Coulomb scattering (MS), energy losses and magnetic field errors. What makes track fits so challenging is the fact that particles in the magnetic fieldd propagate along complex trajectories, which are highly non-linear. For track reconstruction, the fit quality is the most important estimator for finding the correct hit combinations. Especially in high-rate experiments, track finding is a major challenge due to large hit combinatorics.

The most commonly used track fit today is the Kálmán filter (KF)[1, 2]. It uses a state vector to parameterize the track, which is updated with each measurement (hit), together with the quality of the track fit. An advantage of the KF is its high flexibility, which allows for a wide range of applications. Nowadays, many experiments employ an extended version of the Kalman Filter (KF) for track reconstruction, known as the combinatorial Kalman filter (CKF), which aims to identify the optimal hit combinations.

The KF, however, also has disadvantages: the algorithm is recursive, and consequently not well suited for parallel computing. This presents a significant challenge for accelerating track reconstruction using modern highly parallel computing hardware. In addition, the KF does not provide the full covariance matrix of all hit positions, complicating its use for track-based detector alignment. Considering that detector resolutions continue to improve with new tracking detector technologies, the software alignment of the detector system becomes increasingly relevant to fully exploit the potential of detectors.

For detector alignment, the General Broken Line (GBL) fit [3, 4] is better suited as it inherently provides the full hit covariance matrix, which is required to determine correlations and allows for the identification of so-called *weak modes*. An example is the Millepede II software tool [5, 6]. The basic concept of the GBL is to linearize an approximate solution and perform the track fit in a local (curvilinear) coordinate system defined by a reference (seed) solution. MS as well as energy losses then show up as kinks in the transformed trajectory. These kinks are minimized along with the hit residuals in the fit. As the GBL is seeded and requires an approximate solution as starting point, it cannot be used for track finding.

The MS triplet fit [7] is an alternative track fit that uses a linearization approach quite similar to the GBL but does not require any seed or approximate solution. Triplets of hits have the advantage that the reference trajectory for the linearization can be easily calculated from the triplet geometry itself, for example in a uniform magnetic field. Furthermore, hit triplets are over-constrained,

allowing the calculation of a triplet quality that can be used to reject fake hit combinations at an early stage of track reconstruction. With single triplets, even a full track reconstruction in a high track multiplicity environment like FCC-hh is possible, as demonstrated in [8].

Because the result of a single triplet fit can be written as a simple function of triplet-specific parameters, and the global track parameters can be calculated from simple sums of local triplet fits, the MS triplet fit is much faster than any other track fit. Its parallelization capability makes the MS triplet fit ideal for parallel computing, for example on graphics processing units (GPUs). However, since hit position errors are not included, the MS triplet fit is restricted to low-momentum tracks, where MS errors are dominant. The MS triplet fit is used by the Mu3e experiment [9], which searches for the decay $\mu \to eee$ using muons decaying at rest. Here, the triplet fit has been implemented for both offline reconstruction [10] and online track reconstruction on a GPU-based event filter [11].

This work presents the General Triplet Track Fit (GTTF), which is an extension of the MS triplet fit ([7]) and takes into account hit uncertainties as well as all correlations between different hit triplets. Therefore, this work also goes beyond Ref.[12], where hit uncertainties in the fit quality calculation were considered for individual triplets, but correlations between different triplets were neglected. Interestingly, the solution of the GTTF can also be given in an analytical closed-form solution, similar to [7].

A major difference between the GTTF and other track fits is the fit input. The Kálmán filter and the GBL use hit positions as input. In contrast, the GTTF uses so-called *triplet parameters* as input, which represent an interface to all kind of tracking detectors and provide a general description of the detector (triplet) geometry, including the hit position errors, the scattering material and the magnetic field. For this reason, the GTTF is universal as the same fitting code can be used for all tracking detectors and for all experiments. Only the triplet parameters are experiment- and triplet-specific.

The most important advantage of GTTF is the ability to perform triplet filtering during track reconstruction. This, together with the ability to perform track fitting of triplets on a parallel computing architecture, offers great potential for accelerating track reconstruction in high particle rate experiments. In addition, the GTTF also provides the hit covariance matrix, making the fit ideal for track-based alignment.

Thanks to the analytical form of the result, the covariance can be directly calculated from the triplet geometries. It is therefore relatively easy to calculate the tracking resolution for a given detector geometry, without the need for extensive simulation studies. This feature greatly simplifies tracking detector design studies for future experiments.

With the triplet concept one can go even one step further; from the triplet geometries simple *tracking scale parameters* can be calculated, which can be used to define different *tracking regimes*, for example *MS dominated* and *hit uncertainty dominated*. Depending on the tracking regime, different numerical optimizations can be used to accelerate track fitting. Furthermore, a tracking regime analysis can also help in identifying weaknesses of tracking detector designs.

The paper is organized as follows. The fit methodology is introduced in Section 2. The formulas for the global triplet track fit are derived in Section 3, first for the general case, and then in the limit of dominant hit position errors and dominant MS errors. Results for local triplet fits are given in Section 4. A detailed analysis of fitting biases as well as mitigation strategies, including a special regularized MS fit with reduced bias, is presented in Section 5. The triplet parameters, which represent the input to the fit, are calculated in Section 6 for the case of a uniform magnetic field. Triplet parameter solutions for other setups (gap spectrometer dipole and other inhomogeneous magnetic fields) are discussed in the appendix. A special solution obtained from MS in a zero magnetic field is als presented in Section 6. Energy loss corrections and track fits including energy losses are described in Section 7. The potential for exploiting parallel computing for track fitting and track reconstruction using the triplet concept is presented in Section 8, and the tracking regime concept is introduced in Section 9. Finally, Section 10 provides a summary.

2. Fit Methodology and Triplet Representation

The track fit aims at fitting the total particle momentum, p, and the hit positions by simultaneously minimizing the MS angles and the hit position shifts. The hit positions are given as shifts with respect to the measured hit positions $\delta\vec{x}_k = \vec{x}_{\text{fit},k} - \vec{x}_{\text{meas},k}$, with k being the hit index. For a given magnetic field, this set of parameters (p and all $\delta\vec{x}_k$) contains the full information about the particle trajectory.

For track fitting, a χ^2 function is defined that includes MS as well as spatial hit uncertainties according to:

$$\chi^2 = \sum_{j=0}^{n_{\text{scatt}}-1} \frac{\theta_{\text{MS},j}^2}{\sigma_{\theta_{\text{MS}},j}^2} + \sum_{j=0}^{n_{\text{scat-1}}} \frac{\phi_{\text{MS},j}^2}{\sigma_{\phi_{\text{MS}},j}^2} + \sum_{k=0}^{n_{\text{hit}}-1} \delta\vec{x}_k^{\,t}\, \vec{\vec{V}}_k^{\,-1}\, \delta\vec{x}_k. \quad (1)$$

The first two sums[1] run over all hit triplets (index j) and describe MS at the n_{scatt} scattering points. Throughout the work, it is assumed that the position of the scatterers agree with the position of the hits (detector layers). Using spherical coordinates, the MS kink is described by polar ($\theta_{\text{MS},j}$) and azimuthal ($\phi_{\text{MS},j}$) angles. The projected

[1] Throughout this work, counting of hits and triplets starts at 0.

MS angles are divided by the corresponding expected errors ($\sigma_{\theta_{\rm MS},j}$ and $\sigma_{\phi_{\rm MS},j}$). The third sum runs over all hits and describes the contribution from the hit position shifts (residuals). For each hit, the hit position error is described by a 3×3 covariance matrix, $\vec{\vec{V}}_k$ (error ellipse[2]).

The kink angles in the MS terms of Equation 1 depend on the total particle momentum, as illustrated in Figure 1. Instead of the particle momentum, p, the 3D curvature, defined by:

$$\kappa := \frac{q\,B}{p}, \tag{2}$$

is used in the following[3]. Note that for an inhomogeneous magnetic field, $B = B(\vec{x})$, κ is position dependent even if total momentum is conserved.

Matter effects are described by two parameters, an MS parameter and an energy loss parameter. For each hit, both parameters are calculated from the effective path length in the tracking layer material. Note that both matter effects have some momentum (energy) dependence. The error of the MS angle, $\sigma_{\rm MS}$, depends on the momentum and velocity of the particle [13, 14]. Assuming that the particle is ultra-relativistic ($v \approx c$), MS is inverse proportional to the momentum

$$\sigma_{\rm MS} \propto \frac{1}{|p|}, \tag{3}$$

and one can define a *MS parameter* according to:

$$b_{\rm MS} = \frac{\sigma_{\rm MS}}{|\kappa|} = \sigma_{\rm MS} \left|\frac{p}{q\,B}\right|. \tag{4}$$

Similarly, an energy loss parameter, ΔE, can be defined for each tracking layer (hit), accounting for the energy loss, for example due to ionization. An advantage of the triplet fit is that both, the momentum and the effective path length can already be derived from the triplet geometry before fitting (see Section 6).

In the following, it is assumed that the total momentum of the particles is conserved. Energy losses are included at a later stage and discussed in Section 7.

2.1. Triplet Parameters

In a magnetic field, the trajectory between two consecutive hits is fully defined by the value of the total momentum[4] . Consequently, the total momentum defines the kink angle $\Delta\psi = (\Delta\theta,\, \Delta\phi)$ for a hit triplet, as shown in Figure 1.

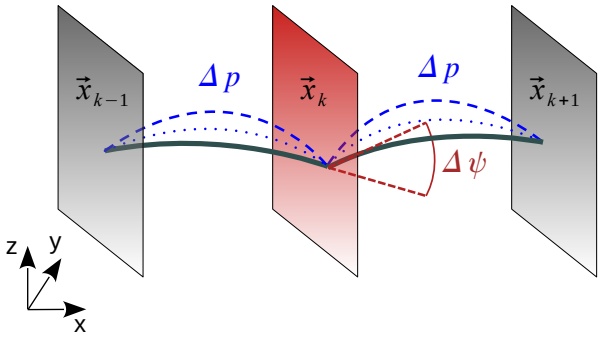

Figure 1: Sketch of the curvature (momentum) dependence of the kink angle in a triplet. The middle plane is the scattering plane in the triplet defined by the hits $\{k-1,\, k,\, k+1\}$. The dashed and dotted trajectories show the momnentum varations of the solid trajectory. The kink angle, indicated at the middle layer, has two projections $\Delta\psi = (\Delta\theta,\, \Delta\phi)$, which are not shown.

Figure 1. Throughout this paper, a right-handed coordinate system is used, with the polar angle, θ, being defined with respect to the z-axis, and the azimuthal angle, ϕ, being defined with respect to the x-axis. The two projections of the kink angle at detector layer k are then defined as:

$$\Delta\theta(p) = \Delta\theta(\kappa) := \theta_{k,k+1} - \theta_{k,k-1}, \tag{5}$$
$$\Delta\phi(p) = \Delta\phi(\kappa) := \phi_{k,k+1} - \phi_{k,k-1}, \tag{6}$$

where the subscript "$k, k-1$" ("$k, k+1$") indicates the particle direction[5] at the detector plane before (after) the scattering at layer k. Both kink angles are functions of the momentum ($\cong$ 3D curvature), and for typical tracking detectors, these functions are transcendental. This is, for example, the case for tracking in a uniform magnetic field or a spectrometer setup. Both cases are discussed in Section 6.

A method for solving the non-linear functions $\Delta\theta(\kappa)$ and $\Delta\phi(\kappa)$, is to perform a linearization around a known solution. Throughout the paper, the solution

$$\Delta\phi_{\rm ref} := \Delta\phi(\kappa_{\rm ref}) = 0 \tag{7}$$

is used as *reference* trajectory, corresponding to no MS in the x-y plane, which is defined to be the *main* bending plane. The reference solution is described by the 3D curvature, $\kappa_{\rm ref}$, and has a non-vanishing polar kink angle $\Delta\theta_{\rm ref} := \Delta\theta(\kappa_{\rm ref})$, in general. The first order linearization around the reference solution then reads:

$$\Delta\phi = 0 + (\kappa - \kappa_{\rm ref})\,\rho_\phi + O(\kappa^2) \approx \tilde{\Phi} + \rho_\phi\,\kappa, \tag{8}$$
$$\Delta\theta = \Delta\theta_{\rm ref} + (\kappa - \kappa_{\rm ref})\,\rho_\theta + O(\kappa^2) \approx \tilde{\Theta} + \rho_\theta\,\kappa\,. \tag{9}$$

The same ansatz was already used in Ref.[7], with the only difference that the linearization was done as function of

[2]Throughout this work, single arrows (double arrows) denote vectors (matrices) in Euclidean space. Furthermore, ^{t} denotes a transposed vector in Euclidean space.

[3]In many other papers, κ is used to denote the transverse curvature, which is henceforth denoted as $\kappa_\perp = q\,B/p_\perp$ in this paper.

[4]Note that there might be no solution for low total momentum tracks, and more than one solution for high momentum tracks, depending on the field configuration.

[5]Note that in uniform magnetic fields the relation $\theta_{k,k'} = \theta_{k',k}$ holds for $k' = k \pm 1$, as the polar angle is an invariant. In contrast, the inequality $\phi_{k,k'} \neq \phi_{k',k}$ generally holds, due to the bending in the magnetic field.

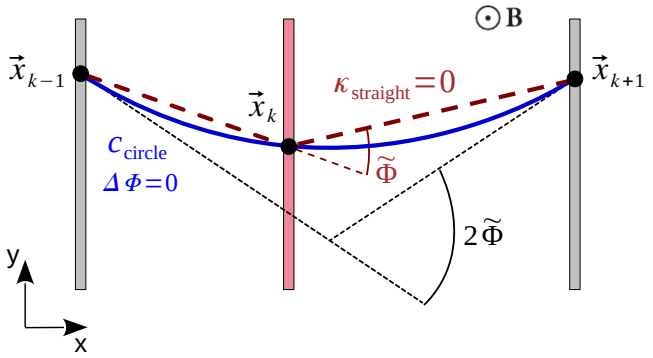

Figure 2: Sketch of a hit triplet in the bending plane of a uniform magnetic field. The *blue solid line* shows the solution for $\Delta\phi = 0$ (zero kink angle); the *brown dashed line* shows the zero curvature solution ($\kappa = 0$). The triplet parameter $\tilde{\Phi}$ corresponds to the kink angle of the zero curvature solution, and is related to the bending angle of the zero kink angle solution via $\Phi_{(\Delta\phi=0)} = 2\,\tilde{\Phi}$.

the 3D radius $R_{3\text{D}} = \kappa^{-1}$, leading to marginally different numerical results for MS fits.

The four linearization parameters $\tilde{\Phi}$, $\tilde{\Theta}$, ρ_ϕ and ρ_θ are *fundamental* parameters, which describe the curvature dependence of the triplet kink angles. In the small bending limit, $\kappa \to 0$, the fundamental triplet parameters $\tilde{\Phi}$ and $\tilde{\Theta}$ can be interpreted as central angle of the hit triplet (see Figure 2 for $\tilde{\Phi}$). The parameter ρ_ϕ is always negative and its absolute value can be interpreted as effective arc lengths of the triplet, as will be shown in Section 6. The parameter ρ_θ is a small correction factor and has no simple geometrical interpretation.

2.2. Representation of Hit Position Errors

In Equation 1, the hit positions and their uncertainties are given in global coordinates. However, using local detector coordinates is often simpler and more intuitive if it comes to hit position uncertainties. Without loss of generality, a transformation into local hit coordinates:

$$\vec{x}_k \to \vec{x}'_k = T_k(\vec{x}_k) \tag{10}$$

is possible, where the position of each hit, k, is described by local bases ($\vec{u}_k$, $\vec{v}_k$, $\vec{w}_k$). In case that the bases are orthogonal, local hit residuals are obtained from the transformation:

$$\vec{\delta}_k = \vec{\vec{Q}}_k \, \Delta\vec{x}_k, \tag{11}$$

with $\Delta\vec{x}_k = \vec{x}_k^{\text{meas}} - \vec{x}_k^{\text{fit}}$ being the hit residuals in global coordinates, and $\vec{\vec{Q}}_k$ being an orthogonal (rotation) matrix[6]. The corresponding covariance matrix in local coordinates is given by:

$$\vec{\vec{V}}'_k = \vec{\vec{Q}}_k \; {}^t \, \vec{\vec{V}}_k \, \vec{\vec{Q}}_k. \tag{12}$$

[6] A transformation into local detector coordinates is highly convenient when the directions of hit position errors are uncorrelated, which is normally the case.

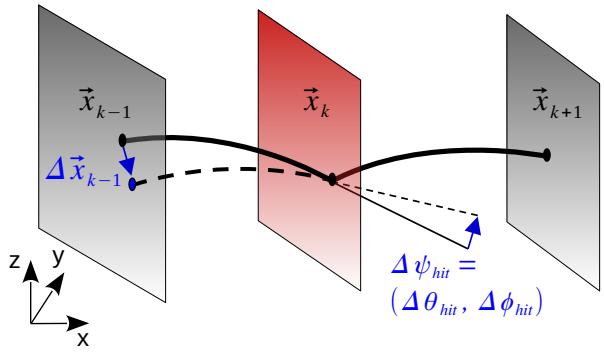

Figure 3: Illustration of the kink angle variation $\Delta\theta_{\text{hit}}$ and $\Delta\phi_{\text{hit}}$ at the scattering layer k for a variation of the hit position in layer $k-1$.

The variation of a hit position leads to a change of the kink angles as shown in Figure 3. In practically all tracking devices, the hit position errors are significantly smaller than the distance between the hits (tracking layers), and the kink angles only weakly depend on the hit positions. The hit position-induced kinks can then be parameterized using the linearization ansatz:

$$\Delta\theta_{\text{hit}} = \sum_{k=0}^{2} \vec{h}_{\theta_k} \, \vec{\delta}_k \;, \tag{13}$$

$$\Delta\phi_{\text{hit}} = \sum_{k=0}^{2} \vec{h}_{\phi_k} \, \vec{\delta}_k \;, \tag{14}$$

with $\vec{h}_{\phi_k}$ and $\vec{h}_{\theta_k}$ being three vectors defined as directional gradients of the three hit positions:

$$\begin{aligned} \vec{h}_{\theta_k} &= \vec{\nabla}_{\vec{\delta}_k} \Delta\theta(\vec{x}_k) \\ &\approx \vec{\nabla}_{\vec{\delta}_k} \tilde{\Theta}(\vec{x}_k) \; + \; \kappa_{\text{ref}} \, \vec{\nabla}_{\vec{\delta}_k} \rho_\theta(\vec{x}_k) \;, \end{aligned} \tag{15}$$

$$\begin{aligned} \vec{h}_{\phi_k} &= \vec{\nabla}_{\vec{\delta}_k} \Delta\phi(\vec{x}_k) \\ &\approx \vec{\nabla}_{\vec{\delta}_k} \tilde{\Phi}(\vec{x}_k) \; + \; \kappa_{\text{ref}} \, \vec{\nabla}_{\vec{\delta}_k} \rho_\phi(\vec{x}_k) \;. \end{aligned} \tag{16}$$

The directional hit gradients can be determined numerically by shifting the hits by 1-sigma of the hit position error into the three orthogonal directions and re-calculating the triplet parameters.

Finally, the MS angles of a triplet entering Equation 1 are expressed as function of the four fundamental triplet parameters, the 3D curvature and the hit position-induced kinks:

$$\theta_{\text{MS}} \;=\; \tilde{\Theta} + \rho_\theta \, \kappa - \Delta\theta_{\text{hit}} \tag{17}$$

$$\phi_{\text{MS}} \;=\; \tilde{\Phi} + \rho_\phi \, \kappa - \Delta\phi_{\text{hit}}. \tag{18}$$

For the general fit of a single triplet, a total of 23 parameters are required. These are the four fundamental triplet parameters, the 3×3 components of the hit gradients, the corresponding hit position errors, and one material parameter. For MS fits where hit uncertainties are neglected, the number of parameters reduces to only five.

3. Global Triplet Track Fit

Using the triplet parameters and the local hit coordinate representation introduced in the last section, the χ^2 function (Equation 1) can be re-written as:

$$\chi^2(\kappa, \vec{\boldsymbol{\delta}}) = \sum_{j=0}^{n_{\text{hit}}-3} \frac{\left(\tilde{\Theta}_j + \rho_{\theta\,j}\,\kappa_j - \Delta\theta_{\text{hit},j}(\vec{\boldsymbol{\delta}})\right)^2}{\sigma^2_{\theta_{\text{MS}},j}} + \sum_{j=0}^{n_{\text{hit}}-3} \frac{\left(\tilde{\Phi}_j + \rho_{\phi\,j}\,\kappa_j - \Delta\phi_{\text{hit},j}(\vec{\boldsymbol{\delta}})\right)^2}{\sigma^2_{\phi_{\text{MS}},j}} + \sum_{k=0}^{n_{\text{hit}}-1} \vec{\delta}_k^{\,t}\, \vec{\vec{V}}_k'^{\,-1}\, \vec{\delta}_k. \quad (19)$$

The fit parameters are the 3D curvature, κ, and the residuals[7] $\vec{\boldsymbol{\delta}} = (\vec{\delta}_0, \vec{\delta}_1, ..., \vec{\delta}_{n_{\text{hit}}-1})^\top$. The 3D curvature, κ is here defined with respect to a reference magnetic field, B_{ref}, according to:

$$\frac{q}{p} = \frac{\kappa}{B_{\text{ref}}} = \frac{\kappa_j}{B_j}, \quad (20)$$

with B_j being the local magnetic field strengths at triplet j. Note that for inhomogeneous magnetic fields, the field dependence of κ can be "absorbed" by the ρ coefficients in Equation 19 by replacing: $\rho_j \to \rho'_j\, B_{\text{ref}}/B_j$. In the following, it is assumed that such an replacement has been made.

In Equation 19, the momentum dependence of the MS uncertainties ($\sigma_{\theta_{\text{MS}}}$ and $\sigma_{\phi_{\text{MS}}}$) is deliberately neglected[8] in order to have at most quadratic terms as function of κ and $\vec{\boldsymbol{\delta}}$. To bring Equation 19 in a more legible form, it is convenient to define two vectors, which contain all fundamental triplet parameters of a track:

$$\boldsymbol{\rho} = (\rho_{\theta_0}, \ \dots\ , \rho_{\theta_{n_{\text{hit}}-3}}; \rho_{\phi_0}, \dots, \rho_{\phi_{n_{\text{hit}}-3}})^\top,$$
$$\tilde{\boldsymbol{\Psi}} = (\tilde{\Theta}_0, \ \dots\ , \tilde{\Theta}_{n_{\text{hit}}-3}; \tilde{\Phi}_0, \ \dots, \ \tilde{\Phi}_{n_{\text{hit}}-3})^\top,$$

and whose length is twice the number of triplets. Moreover, *precision matrices* are defined for MS and hit position errors:

$$\boldsymbol{D}_{\text{MS}} = \mathbf{diag}\left(\frac{1}{\sigma^2_{\theta_{\text{MS}},0}}, \ \dots\ , \frac{1}{\sigma^2_{\theta_{\text{MS}},n_{\text{hit}}-3}}; \frac{1}{\sigma^2_{\phi_{\text{MS}},0}}, \ \dots\ , \frac{1}{\sigma^2_{\phi_{\text{MS}},n_{\text{hit}}-3}}\right),$$
$$\vec{\vec{\boldsymbol{D}}}_{\text{hit}} = \mathbf{diag}\left(\vec{\vec{V}}_0'^{\,-1}, \ \vec{\vec{V}}_1'^{\,-1}, \ \dots\ , \ \vec{\vec{V}}_{n_{\text{hit}}-1}'^{\,-1}\right).$$

[7] Here (and in the following), bold symbols refer to vectors (lowercase variables) and matrices (uppercase variables), either in hit or triplet space. Furthermore, within this work two different transposition signs are used. The ^{t} operator acts on Euclidean space, whereas the $^\top$ operator acts on both triplet and hit space, also including all directions of the hit position errors.

[8] Neglecting the momentum dependence by setting σ_{MS} constant, leads to a small momentum bias in track fits for MS-dominated particles, see also Section 5.

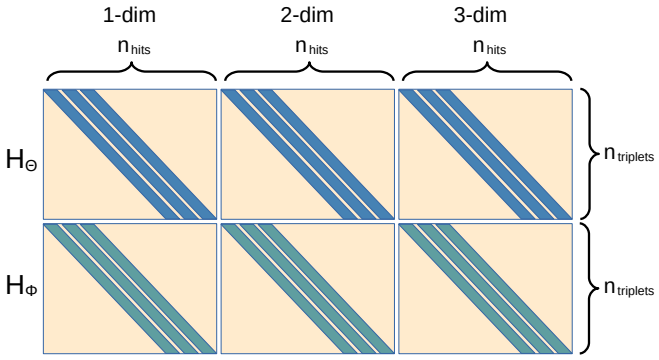

Figure 4: Sketch of the rectangular matrix $\vec{\boldsymbol{H}}$. The horizontal block structure originates from the three directions of the hit position errors. The vertical block structure originates from the two projections of the MS angular error. Only elements in the blue and turquoise bands, which originate from the three hits contributing to a triplet, are non-zero.

$\boldsymbol{D}_{\text{MS}}$ and $\vec{\vec{\boldsymbol{D}}}_{\text{hit}}$ are diagonal matrices, whose ranks are $2\,n_{\text{triplet}}$ and $3\,n_{\text{hits}}$, respectively. Elements in the MS precision matrix $\boldsymbol{D}_{\text{MS}}$ are partially related, since:

$$\sigma_{\theta_{\text{MS}},j} = \sigma_{\text{MS},j}, \quad (21)$$
$$\sigma_{\phi_{\text{MS}},j} = \sigma_{\text{MS},j}/\sin\hat{\theta}_j, \quad (22)$$

with $\sigma_{\text{MS},j}$ being the MS angular error (Equation 3) of the j^{th} triplet and $\hat{\theta}_j$ being the corresponding estimated average polar angle in the MS process. The $1/\sin\hat{\theta}_j$ factor in Equation 22 is a geometrical factor originating from the chosen spherical coordinate representation. Note that the $1/\sin\hat{\theta}_j$ term is treated as a constant, since it enters only as a weighting factor to the fit and the corresponding propagated polar angle uncertainties are negligible.

To collect all hit gradients, defined by Equation 15 and Equation 16, a hit gradient matrix (Jacobian) is defined, according to:

$$\vec{\boldsymbol{H}} := \left(\vec{\boldsymbol{h}}_\theta^{(0)}, \ \dots\ , \vec{\boldsymbol{h}}_\theta^{(n_{\text{hit}}-3)}; \vec{\boldsymbol{h}}_\phi^{(0)}, \ \dots\ , \vec{\boldsymbol{h}}_\phi^{(n_{\text{hit}}-3)}\right)^\top,$$

where the vectors $\vec{\boldsymbol{h}}_\theta^{(j)}$ and $\vec{\boldsymbol{h}}_\phi^{(j)}$ are defined in hit-space and collect all hit gradients of triplet j:

$$\vec{\boldsymbol{h}}_\theta^{(j)} := \left(\vec{h}^{(j)}_{\theta_0}, \vec{h}^{(j)}_{\theta_1}, \dots, \vec{h}^{(j)}_{\theta_{n_{\text{hit}}-1}}\right),$$
$$\vec{\boldsymbol{h}}_\phi^{(j)} := \left(\vec{h}^{(j)}_{\phi_0}, \vec{h}^{(j)}_{\phi_1}, \dots, \vec{h}^{(j)}_{\phi_{n_{\text{hit}}-1}}\right).$$

Note that only elements with the indices $k = j,\ j+1,\ j+2$ (this are the hits forming the triplet) are non-zero. The matrix $\vec{\boldsymbol{H}}$ has in total $2\,n_{\text{triplet}} \times 3\,n_{\text{hit}}$ components; its structure is sketched in Figure 4.

The χ^2 function (Equation 19) then reads in compact form:

$$\chi^2(\kappa,\vec{\boldsymbol{\delta}}) \;=\; \left(\boldsymbol{\Psi}+\boldsymbol{\rho}\,\kappa-\vec{\boldsymbol{H}}\vec{\boldsymbol{\delta}}\right)^{\top}\boldsymbol{D}_{\mathrm{MS}}\,\left(\boldsymbol{\Psi}+\boldsymbol{\rho}\,\kappa-\vec{\boldsymbol{H}}\vec{\boldsymbol{\delta}}\right) \;+\; \vec{\boldsymbol{\delta}}^{\top}\vec{\boldsymbol{D}}_{\mathrm{hit}}\,\vec{\boldsymbol{\delta}}. \tag{23}$$

Minimizing Equation 23 results in a system of linear equations:

$$\begin{pmatrix} -\boldsymbol{\rho}^{\top}\boldsymbol{D}_{\mathrm{MS}}\,\vec{\boldsymbol{\Psi}} \\ \vec{\boldsymbol{H}}^{\top}\boldsymbol{D}_{\mathrm{MS}}\,\vec{\boldsymbol{\Psi}} \end{pmatrix} \;= \tag{24}$$
$$\begin{pmatrix} \boldsymbol{\rho}^{\top}\boldsymbol{D}_{\mathrm{MS}}\,\boldsymbol{\rho} & -\boldsymbol{\rho}^{\top}\boldsymbol{D}_{\mathrm{MS}}\,\vec{\boldsymbol{H}} \\ -\vec{\boldsymbol{H}}^{\top}\boldsymbol{D}_{\mathrm{MS}}\,\boldsymbol{\rho} & \vec{\boldsymbol{D}}_{\mathrm{hit}}+\vec{\boldsymbol{H}}^{\top}\boldsymbol{D}_{\mathrm{MS}}\,\vec{\boldsymbol{H}} \end{pmatrix} \begin{pmatrix} \kappa \\ \vec{\boldsymbol{\delta}} \end{pmatrix} .$$

Solving the system above yields for the 3D curvature and its variance:

$$\kappa_{\mathrm{min}} \;=\; -\frac{\boldsymbol{\rho}^{\top}\boldsymbol{K}\boldsymbol{\Psi}}{\boldsymbol{\rho}^{\top}\boldsymbol{K}\boldsymbol{\rho}}, \tag{25}$$

$$\sigma^2_{\kappa_{\mathrm{min}}} \;=\; \frac{1}{\boldsymbol{\rho}^{\top}\boldsymbol{K}\boldsymbol{\rho}}, \tag{26}$$

with $\boldsymbol{K}$ being the *triplet precision matrix*. Its inverse, the covariance matrix, is defined as:

$$\boldsymbol{K}^{-1} \;=\; \boldsymbol{D}^{-1}_{\mathrm{MS}} \;+\; \vec{\boldsymbol{H}}\vec{\boldsymbol{D}}^{-1}_{\mathrm{hit}}\vec{\boldsymbol{H}}^{\top}. \tag{27}$$

$\boldsymbol{K}^{-1}$ combines the MS and hit position covariance matrices and is called *triplet covariance matrix*. Inversion of the triplet covariance matrix is trivial in case of dominant MS errors since $\boldsymbol{D}^{-1}_{\mathrm{MS}}$ is diagonal (see also Section 3.2). The inversion is more involved if spatial hit uncertainties contribute. Note that the matrix $\vec{\boldsymbol{H}}\vec{\boldsymbol{D}}^{-1}_{\mathrm{hit}}\vec{\boldsymbol{H}}^{\top}$ has a 2×2 block structure with penta-diagonal sub-matrices.[9]

The residuals and the corresponding covariance matrix are calculated as:

$$\vec{\boldsymbol{\delta}}_{\mathrm{min}} \;=\; \vec{\boldsymbol{D}}^{-1}_{\mathrm{hit}}\vec{\boldsymbol{H}}^{\top}\,\boldsymbol{K}_{\boldsymbol{\rho}}\,\boldsymbol{\Psi}, \tag{28}$$

$$\vec{\mathbf{Cov}}_{\delta_{\mathrm{min}}} \;=\; \vec{\boldsymbol{D}}^{-1}_{\mathrm{hit}} - \vec{\boldsymbol{D}}^{-1}_{\mathrm{hit}}\vec{\boldsymbol{H}}^{\top}\,\boldsymbol{K}_{\boldsymbol{\rho}}\,\vec{\boldsymbol{H}}\,\vec{\boldsymbol{D}}^{-1}_{\mathrm{hit}}, \tag{29}$$

with

$$\boldsymbol{K}_{\boldsymbol{\rho}} \;=\; \left(\boldsymbol{K}-\frac{\boldsymbol{K}\boldsymbol{\rho}\boldsymbol{\rho}^{\top}\boldsymbol{K}}{\boldsymbol{\rho}^{\top}\boldsymbol{K}\boldsymbol{\rho}}\right). \tag{30}$$

Note that the matrix $\boldsymbol{K}_{\boldsymbol{\rho}}$ only exists for $\det(\boldsymbol{K})\neq 0$.

Finally, the fit quality is given by:

$$\begin{aligned}\chi^2_{\mathrm{min}} \;&=\; \boldsymbol{\Psi}^{\top}\boldsymbol{K}\boldsymbol{\Psi} \;-\; \frac{(\boldsymbol{\rho}^{\top}\boldsymbol{K}\boldsymbol{\Psi})^2}{\boldsymbol{\rho}^{\top}\boldsymbol{K}\boldsymbol{\rho}} \\ &=\; \boldsymbol{\Psi}^{\top}\boldsymbol{K}_{\boldsymbol{\rho}}\boldsymbol{\Psi}.\end{aligned} \tag{31}$$

[9] The penta-diagonal structure of the sub-matrices can be exploited for large matrices where the computational effort for the inversion scales linearly with the number of hits (tracking layers).

The first term in the first line accounts for the kink angles of the infinite momentum solution whereas the second term describes the improvement of the fit quality by fitting the hit positions and the 3D curvature. The second line of Equation 31 suggests that $\boldsymbol{K}_{\boldsymbol{\rho}}$ can be interpreted as post-fit precision matrix for the kink angles.

Note that with Equation 25, and Equation 28 the trajectory is fully determined from the first to the last hit.

3.1. Global Fit for Dominant Hit Position Errors

In the limit of dominating hit position errors, the MS errors can be neglected: $||\boldsymbol{D}_{\mathrm{MS}}||^{-1}\rightarrow 0$. The solution looks very similar to the general case discussed above, and is given in Appendix A, for completeness.

3.2. Global Fit for Dominant MS Errors

In the case of dominant MS errors, the hit position errors can be neglected. By replacing the triplet covariance matrix by the MS covariance matrix, $\boldsymbol{K}\rightarrow\boldsymbol{D}_{\mathrm{MS}}$, one obtains for the curvature and its variance:

$$\kappa_{\mathrm{MS}} \;=\; -\frac{\boldsymbol{\rho}^{\top}\boldsymbol{D}_{\mathrm{MS}}\,\boldsymbol{\Psi}}{\boldsymbol{\rho}^{\top}\boldsymbol{D}_{\mathrm{MS}}\,\boldsymbol{\rho}}, \tag{32}$$

$$\sigma^2_{\kappa_{\mathrm{MS}}} \;=\; \frac{1}{\boldsymbol{\rho}^{\top}\boldsymbol{D}_{\mathrm{MS}}\,\boldsymbol{\rho}}, \tag{33}$$

and for the fit quality:

$$\chi^2_{\mathrm{MS}} \;=\; \boldsymbol{\Psi}^{\top}\boldsymbol{D}_{\mathrm{MS}}\,\boldsymbol{\Psi} \;-\; \frac{(\boldsymbol{\rho}^{\top}\boldsymbol{D}_{\mathrm{MS}}\,\boldsymbol{\Psi})^2}{\boldsymbol{\rho}^{\top}\boldsymbol{D}_{\mathrm{MS}}\,\boldsymbol{\rho}}. \tag{34}$$

Due to the diagonal form of $\boldsymbol{D}_{\mathrm{MS}}$, the global track curvature and the fit quality can be written as simple error-weighted sums of local triplet quantities:

$$\kappa_{\mathrm{MS}} \;=\; \sigma^2_{\kappa_{\mathrm{MS}}}\sum_{j=0}^{n_{\mathrm{triplet}}-1}\frac{{\kappa_{\mathrm{MS},j}}^2}{\sigma^2_{\kappa_{\mathrm{MS},j}}}, \tag{35}$$

$$\frac{1}{\sigma^2_{\kappa_{\mathrm{MS}}}} \;=\; \sum_{j=0}^{n_{\mathrm{triplet}}-1}\frac{1}{\sigma^2_{\kappa_{\mathrm{MS},j}}}, \tag{36}$$

$$\chi^2_{\mathrm{MS}} \;=\; \sum_{j=0}^{n_{\mathrm{triplet}}-1}\chi^2_{\mathrm{MS},j} \;+\; \sum_{j=0}^{n_{\mathrm{triplet}}-1}\frac{(\kappa_{\mathrm{MS}}-\kappa_{\mathrm{MS},j})^2}{\sigma^2_{\kappa_{\mathrm{MS},j}}}, \tag{37}$$

where the indexed parameters denote the results obtained from the local triplet fits, which can be given in analytical closed-form (see Section 4). Note that the fit quality (Equation 37) has two terms: a sum over the individual triplet qualities and a weighted sum over the curvature residuals (curvature consistency term[10]).

[10] The combination of triplets using the MS fit was first discussed in Ref.[7] (Equation 39 therein) where, however, the curvature consistency term is not given.

Fit Quality Relations

For dominant MS errors, the following inequality can be derived from Equation 37:

$$\chi^2_{\mathrm{MS}} \geq \sum_{j=0}^{n_{\mathrm{triplet}}-1} \chi^2_{\mathrm{MS},j}. \tag{38}$$

By summing up the individual triplet fit qualities an lower limit on the global track fit quality is obtained. Equation 38 can therefore be used to reject bad track candidates already at triplet level, thus accelerating track reconstruction.

The fit quality of the MS fit is also related to the quality of the general fit:

$$\chi^2_{\mathrm{min}} \;=\; \chi^2_{\mathrm{MS}} \;+\; \frac{(\kappa_{\mathrm{min}} - \kappa_{\mathrm{MS}})^2}{\sigma_{\kappa_{\mathrm{MS}}}} \;-\; \vec{\boldsymbol{\delta}}^{\top}_{\mathrm{min}} \vec{\vec{\boldsymbol{P}}}\, \vec{\boldsymbol{\delta}}_{\mathrm{min}}, \tag{39}$$

with

$$\vec{\vec{\boldsymbol{P}}} \;=\; \vec{\boldsymbol{H}}^{\top} \boldsymbol{D}_{\mathrm{MS}}\, \vec{\boldsymbol{H}} + \vec{\vec{\boldsymbol{D}}}_{\mathrm{hit}} \tag{40}$$

being the *adjoint triplet precision matrix*[11], which has the rank $3n_{\mathrm{hit}}$. As non-zero hit residuals can only result from a χ^2-improvement, the MS fit quality poses an upper limit for the general fit quality:

$$\chi^2_{\mathrm{min}} \;\leq\; \chi^2_{\mathrm{MS}}. \tag{41}$$

This relation is of high relevance for fast track finding: Since the computational effort for the MS fit is significantly lower than for the general fit, which involves matrix inversion, it is often advantageous to perform the MS fit first, see discussion in Section 9.

3.3. Large Hit Position Uncertainties

Results obtained with GTTF linearization ansatz (Equation 8 and Equation 9 are only valid if the hit position uncertainties are small compared to the distance of track layers, and so-called *rotational triplet uncertainties* can be neglected. However, these rotational uncertainty can be significant for strip detectors. Correction factors to include this uncertainty are given in Appendix C.

3.4. Track Parameters For Track Extrapolation

The output of the GTTF are the curvature (momentum) and all hit residuals. These parameters define the full trajectory, from the first to the last hit. For track extrapolation or vertexing, also the track direction and the corresponding covariance matrix need to be known. Both are position depend and, in general, complicated functions of the hit positions and the curvature.

For the special case of a uniform magnet field, the calculation of all track parameters and the corresponding covariance matrix is shown in Appendix D. The track parameter calculation is very similar for other magnetic field configurations.

[11] The triplet precision matrix $\boldsymbol{K}$ and the adjoint triplet precision matrix $\boldsymbol{P}$ are related by: $\vec{\vec{\boldsymbol{P}}}^{-1} \vec{\boldsymbol{H}}^{\top} \boldsymbol{D}_{\mathrm{MS}} = \vec{\vec{\boldsymbol{D}}}^{-1}_{\mathrm{hit}} \vec{\boldsymbol{H}}^{\top} \boldsymbol{K}$.

3.5. Additional Material in Tracking Volume

Additional material, which affects the particle tracjectory by MS or energy loss, can be easily included in the GTTF by introducing so-called *pseudo-hits* in *pseudo-tracking* layers. Pseudo-hits can be calculated by intersecting an already existing, approximate solution of the trajectory with the material layer, and by assigning (sufficiently) large hit position uncertainties. It can be easily proven that the fit result remains stable as the hit uncertainties in the pseudo-tracking layers approach infinity.

4. Local Triplet Fit

The local triplet fit represents the simplest solution of the GTTF, and is highly relevant for seeding track reconstruction and filtering. The solution is readily obtained from Equations 25 to 31. For a triplet, the covariance matrix, $\boldsymbol{K}^{-1}$, reduces to a 2×2 matrix. The elements of this local covariance matrix, defined as

$$\boldsymbol{K}^{-1}_{\mathrm{loc}} \;=\; \begin{pmatrix} \Gamma_{\theta\theta}{}^{\star} & \Gamma_{\theta\phi} \\ \Gamma_{\theta\phi} & \Gamma_{\phi\phi}{}^{\star} \end{pmatrix}, \tag{42}$$

are given by:

$$\begin{aligned} \Gamma_{\theta\theta}{}^{\star} &:= \Gamma_{\theta\theta} \;+\; \sigma^2_{\theta_{\mathrm{MS},k}} \\ &:= \sum_{k \,\in\, \mathrm{triplet}} \vec{h}^{\,t}_{\theta_k} \vec{\vec{V}}'_k\, \vec{h}_{\theta_k} \;+\; \sigma^2_{\theta_{\mathrm{MS},k}}\,, \end{aligned} \tag{43}$$

$$\begin{aligned} \Gamma_{\phi\phi}{}^{\star} &:= \Gamma_{\phi\phi} \;+\; \sigma^2_{\phi_{\mathrm{MS},k}} \\ &:= \sum_{k \,\in\, \mathrm{triplet}} \vec{h}^{\,t}_{\phi_k} \vec{\vec{V}}'_k\, \vec{h}_{\phi_k} \;+\; \sigma^2_{\phi_{\mathrm{MS},k}}\,, \end{aligned} \tag{44}$$

$$\Gamma_{\theta\phi} := \sum_{k \,\in\, \mathrm{triplet}} \vec{h}^{\,t}_{\theta_k} \vec{\vec{V}}'_k\, \vec{h}_{\phi_k}\,. \tag{45}$$

The solution of the local triplet fit is a function of those Γ parameters, and the 3D curvature and its variance are given by:

$$\begin{aligned} \kappa_{\mathrm{loc}} \;&= \\ &- \frac{\tilde{\Theta}\,\rho_\theta\,\Gamma_{\phi\phi}{}^{\star} \;+\; \tilde{\Phi}\,\rho_\phi\,\Gamma_{\theta\theta}{}^{\star} \;-\; \Gamma_{\theta\phi}\,(\tilde{\Phi}\rho_\theta + \tilde{\Theta}\rho_\phi)}{\rho^2_\theta\,\Gamma_{\phi\phi}{}^{\star} \;+\; \rho^2_\phi\,\Gamma_{\theta\theta}{}^{\star} \;-\; 2\rho_\theta\,\rho_\phi\,\Gamma_{\theta\phi}}, \end{aligned} \tag{46}$$

$$\sigma^2_{\kappa_{\mathrm{loc}}} \;=\; \frac{\Gamma_{\theta\theta}{}^{\star}\,\Gamma_{\phi\phi}{}^{\star} - \Gamma_{\theta\phi}{}^2}{\rho^2_\theta\,\Gamma_{\phi\phi}{}^{\star} \;+\; \rho^2_\phi \Gamma_{\theta\theta}{}^{\star} \;-\; 2\rho_\phi\,\rho_\theta \Gamma_{\theta\phi}}. \tag{47}$$

For the local fit quality, one obtains:

$$\chi^2_{\mathrm{loc}} \;=\; \frac{(\tilde{\Theta}\rho_\phi - \tilde{\Phi}\rho_\theta)^2}{\rho^2_\theta\,\Gamma_{\phi\phi}{}^{\star} \;+\; \rho^2_\phi\,\Gamma_{\theta\theta}{}^{\star} \;-\; 2\rho_\phi\,\rho_\theta\,\Gamma_{\theta\phi}}. \tag{48}$$

Furthermore, the residual vector of hit k is given by:

$$\vec{\delta}_{k,\mathrm{loc}} \;=\; \vec{\vec{V}}'_k\, \frac{(\rho_\theta\, \vec{h}_{\phi_k} - \rho_\phi\, \vec{h}_{\theta_k})}{(\rho_\theta \tilde{\Phi} - \rho_\phi \tilde{\Theta})}\, \chi^2_{\mathrm{loc}}. \tag{49}$$

The covariance matrix of the residuals can be written as:

$$\vec{\mathbf{C}}\mathbf{ov}_{\boldsymbol{\delta}} \;=\; \vec{\boldsymbol{D}}_{\text{hit}}^{-1} \;-\; \frac{\vec{\boldsymbol{\delta}}_{\text{loc}}\,\vec{\boldsymbol{\delta}}_{\text{loc}}^{\top}}{\chi^2}. \tag{50}$$

The first term in Equation 50 contains the pre-fit hit position errors, whereas the second term describes their improvement by the track fit.

Special Cases for Local Triplet Fits

In the case of dominant hit position errors, the following substitutions are applicable:

$$\Gamma_{\theta\theta}{}^{\star} \to \Gamma_{\theta\theta}, \tag{51}$$
$$\Gamma_{\phi\phi}{}^{\star} \to \Gamma_{\phi\phi}. \tag{52}$$

In other words, one obtains the same fitting formulas as for the general triplet fitting by simply removing the * from all equations.

For dominant MS errors, the following substitutions are applicable:

$$\Gamma_{\theta\theta}{}^{\star} \to \sigma^2_{\theta_{MS}} \tag{53}$$
$$\Gamma_{\phi\phi}{}^{\star} \to \sigma^2_{\phi_{MS}} \tag{54}$$
$$\Gamma_{\theta\phi} \to 0, \tag{55}$$

and the local triplet fit formulas (Equation 46 to Equation 48) further simplify. The hit residuals (Equation 49) vanish by definition and the 3D curvature (Equation 46 simplifies to:

$$\kappa_{\text{MS}} \;=\; -\,\frac{\rho_\phi\;\tilde{\Phi}\;\sin^2\hat{\theta} + \rho_\theta\;\tilde{\Theta}}{\rho_\phi^2\;\sin^2\hat{\theta} + \rho_\theta^2}, \tag{56}$$

Note that Equation 56 is independent of the angular MS error, and therefore does not depend on the amount of material at the scattering layer.

5. Momentum Bias in Track Fits

The tracking model used by the GTTF and other standard fits, such as the Kálmán Filter and General Broken Lines, is the same; they all include hit position and MS uncertainties. The only difference is the way how the tracking model is implemented or how linearizations are performed.

Due to the momentum dependence of the MS uncertainty, see Equation 3, a fitting bias towards higher momenta (smaller curvatures) naturally arises in all track fits. The reason is that the *estimated* MS angular errors ($\sigma_{\theta_{\text{MS}}}$ and $\sigma_{\phi_{\text{MS}}}$ in Equation 1) are smaller for high momentum tracks than for low-momentum tracks. This bias is an inherent property of track fits that include MS uncertainties and where the particle momentum is a fit parameter.

The analytical form of the GTTF solution facilitates the study of fitting biases. Below, a detailed study of fitting biases is presented and a method for bias mitigation is proposed.

5.1. Curvature Pull Distribution

One way to check the goodness of a fit is by studying the pull distributions of the fitted parameters. The curvature pull for fit i is defined as:

$$\mathrm{g}(\kappa)_i \;=\; \frac{\kappa_i - \kappa^{\text{true}}}{\sigma_{\kappa,i}}. \tag{57}$$

For a fit with statistically correct estimates of κ and σ_κ, the arithmetic mean of the pull distribution is expected to vanish, $\mathbb{E}[\mathrm{g}(\kappa)] = 0$, and the variance is expected to be unity, $\mathrm{Var}[\mathrm{g}(\kappa)] = 1$. In the following, the pull distribution is studied for the Local Track Fit and the Global Track Fit in a scenario where MS errors dominate.

5.1.1. Curvature Pull in the Local Track Fit

For a single triplet, the curvature pull can be calculated by smearing the particle momentum with a Gaussian distribution and recalculating the curvature error from the smeared quantity. For small curvature errors, i.e., $\sigma_\kappa^2 \ll \kappa^2$, one obtains:

$$\mathbb{E}[\mathrm{g}(\kappa)] \approx\; -\frac{|\sigma_{\kappa_{\text{MS}}}|}{\kappa}. \tag{58}$$

The expected curvature pull is shifted toward smaller curvatures (corresponding to higher momenta). It is interesting to note that the curvature itself is correctly fitted, i.e., $\mathbb{E}[\kappa] = \kappa^{\text{true}}$. Since the bias of the curvature pull distribution is caused by the *a priori* unknown MS uncertainty, this effect is henceforth referred to as *MS normalization bias*.

5.1.2. Curvature Pull in Global Triplet Track Fit

For dominant MS angular errors, the 3D curvature in the global fit becomes a weighted sum of the local triplet fits (see Section 3.2). Due to the MS normalization bias discussed in the previous section, high momentum triplets receive a higher weight in the fit than low-momentum triplets. This leads to the so-called *weighting bias* of the curvature.

For demonstration, the weighting bias has been studied for a simple detector geometry with equidistant tracking layers. Using a toy Monte Carlo, the following relation was empirically found for the weighting bias:

$$\mathbb{E}[\kappa] - \kappa^{\text{true}} = \;-\left(2 - \frac{2}{n_{\text{triplet}}}\right)\frac{\sigma^2_{\kappa_{\text{MS}}}}{\kappa^{\text{true}}}. \tag{59}$$

with n_{triplet} being the number of triplets combined. The weighting bias depends quadratically on the curvature error and is negative.

All together, the pull distribution (Equation 57) is influenced by two effects: the weighting bias, which leads to a shift in the curvature, and the MS normalization bias, which creates an asymmetry in the pull distribution.

5.2. Bias Mitigation in the Global Triplet Fit

The size of the bias depends on the accuracy with which the MS uncertainties are known prior to the fit. For the global fit, there are several options to calculate the MS angular errors that enter the MS precision matrix $\boldsymbol{D}_{\mathrm{MS}}$ (listed in order of increasing precision):

- from triplet parameter based estimates of the curvature (momentum), for example using the simple relation: $\kappa^{\mathrm{est}} = \tilde{\Phi}/\rho_{\phi}$,
- from locally fitted curvatures derived before the global fit, $\kappa^{\mathrm{est}} = \kappa_{\mathrm{loc}}$ (Equation 46),
- by repeating ("updating") the global fit (Equation 25 or Equation 32), where the MS angular errors are calculated from the curvature obtained in the first fit: $\kappa^{\mathrm{est}} = \kappa_{\mathrm{global}}(1^{\mathrm{st}}\ \mathrm{fit})$[12].

Since the global fit has a significantly higher precision than the local fits, the bias is significantly reduced by using the third method. The downside is that the precision matrix $\boldsymbol{K}$ must be re-calculated (matrix inversion) after updating the MS angular errors, essentially doubling the computational effort.

Note that the same fitting bias also occurs in the KF. However, due to the gradually increasing momentum precision, the bias in the KF in smaller compared to the GTTF without updating. After the final smoothing step (KF) and update of the MS uncertainties (GTTF), the fitting biases of both methods are expected to be identical, as they use the same MS uncertainties as input for the track fit.

5.3. Regularized MS Fit

The weighting bias of the curvature can be reduced by explicitly including the momentum dependence of the MS angular errors (Equation 3) in the fit. If included, minimization of the general χ^2 formula (Equation 19) yields a system of equations that contains non-linear $\kappa^2 \cdot \delta_k$ terms, which is difficult to solve. However, since the bias is mainly relevant for the case of prevailing MS errors, hit position errors are ignored in the following. The MS precision matrix can then be replaced by a new matrix that depends only on the MS parameters, defined in Equation 4:

$$\boldsymbol{D}_{\mathrm{MS}} \rightarrow \frac{1}{\kappa^2}\boldsymbol{B}_{\mathrm{MS}}, \qquad \text{with}$$

$$\boldsymbol{B}_{\mathrm{MS}} := \mathbf{diag}\left(\frac{1}{b^2_{\mathrm{MS},0}}, \ldots, \frac{1}{b^2_{\mathrm{MS},n_{\mathrm{hit}}-3}}; \frac{\sin^2\hat{\theta}_0}{b^2_{\mathrm{MS},0}}, \ldots, \frac{\sin^2\hat{\theta}_{n_{\mathrm{hit}}-3}}{b^2_{\mathrm{MS},n_{\mathrm{hit}}-3}}\right).$$

[12] The updating of the GTTF corresponds to the *smoothing* step of the KF.

The fit quality after linearization then reads in compact form:

$$\chi^2_{\mathrm{MSreg}}(\kappa) = \frac{(\boldsymbol{\Psi} + \boldsymbol{\rho}\,\kappa)^{\top}\,\boldsymbol{B}_{\mathrm{MS}}\,(\boldsymbol{\Psi} + \boldsymbol{\rho}\,\kappa)}{\kappa^2}, \tag{60}$$

and minimization of above equation yields:

$$\kappa_{\mathrm{MSreg}} = -\frac{\boldsymbol{\Psi}^{\top}\boldsymbol{B}_{\mathrm{MS}}\,\boldsymbol{\Psi}}{\boldsymbol{\rho}^{\top}\boldsymbol{B}_{\mathrm{MS}}\,\boldsymbol{\Psi}}, \tag{61}$$

$$\sigma^2_{\kappa_{\mathrm{MSreg}}} = \frac{(\boldsymbol{\Psi}^{\top}\boldsymbol{B}_{\mathrm{MS}}\,\boldsymbol{\Psi})^3}{(\boldsymbol{\rho}^{\top}\boldsymbol{B}_{\mathrm{MS}}\,\boldsymbol{\Psi})^4}. \tag{62}$$

Finally, the fit quality is given by:

$$\chi^2_{\mathrm{MSreg}} = \boldsymbol{\rho}^{\top}\boldsymbol{B}_{\mathrm{MS}}\,\boldsymbol{\rho} - \frac{(\boldsymbol{\rho}^{\top}\boldsymbol{B}_{\mathrm{MS}}\,\boldsymbol{\Psi})^2}{\boldsymbol{\Psi}^{\top}\boldsymbol{B}_{\mathrm{MS}}\,\boldsymbol{\Psi}}. \tag{63}$$

For completeness, formulas for the regularized local triplet fit are given in Appendix B.

The regularized MS fit has the advantage that the curvature pull distribution is free of bias, see Section 5.4. Another advantage is that the fit depends only on the MS parameters ($\boldsymbol{B}_{\mathrm{MS}}$), and no longer on the estimated MS errors ($\boldsymbol{D}_{\mathrm{MS}}$). Therefore, there is no need to estimate the MS angular error before (global) fitting.

5.4. Comparison of Regularized and Unregularized MS Fits

The biases of the regularized and unregularized MS fit are quantitatively compared using an example: A relativistic particle with a momentum of 300 MeV/c is simulated in a uniform magnetic field of 3 T using three tracking layers over a total distance of 60 mm. The material thickness of the middle tracking layer corresponds to 2 % X_0. Assuming that hit position errors are negligible, the corresponding relative curvature (momentum) resolution of this setup is about 23 %.

A comparison of the two fits reveals contrasting results: For $n_{\mathrm{triplet}} = 1$, the unregularized MS fit has a mean curvature pull of -25 % (towards higher momenta), see Figure 5, which further increases if more triplets are combined. The regularized MS fit has no pull, as expected. The negative curvature pull of the unregularized MS fit is a combined effect of the MS normalization bias (Section 5.1.1) and the weighting bias (Section 5.1.2), which can be described by a function that adds both sources quadratically, resulting in:

$$\mathbb{E}[g_{\kappa}] = -\sqrt{\frac{8n^2 - 5n + 4}{n}}\,\frac{\sigma_{\kappa_{\mathrm{MS}}}}{\kappa^{\mathrm{true}}}, \tag{64}$$

As shown in Figure 5, Equation 64 describes the simulation data reasonably well.

In Figure 6, the curvature bias of both fits is shown. For $n_{\mathrm{triplet}} = 1$, the unregularized MS fit has no curvature bias. However, the regularized MS fit has a relative bias of +5 % (towards lower momenta). This positive curvature bias compensates for the negative normalization bias, so

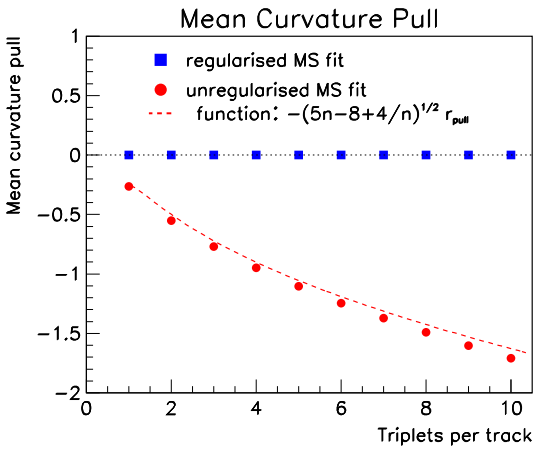

Figure 5: Simulated mean curvature pull (Equation 57) as function of the number of triplets for a relative curvature (momentum) resolution of 23 %. The results are shown for regularized (*blue squares*) and unregularized (*red points*) MS fits. The statistical errors are of the order of 1 per mil. The data points are compared with empirical functions. See text for more explanation.

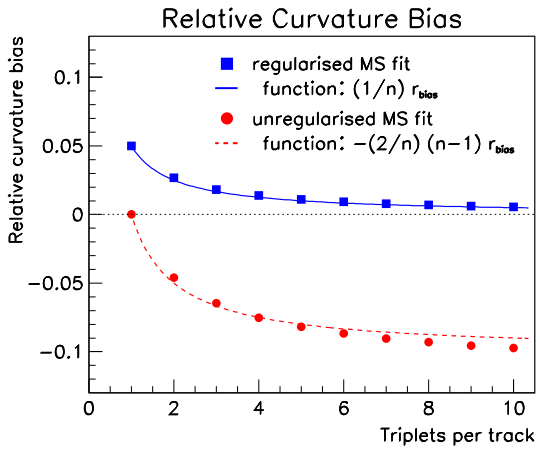

Figure 6: Simulated relative bias of the curvature, $\mathbb{E}[\kappa_{\text{MSreg}}]/\kappa^{\text{true}} - 1$, as a function of the number of triplets per track for a relative curvature (momentum) resolution of 23 %. For more information, see caption of Figure 5.

that the pull distribution of the regularized MS fit is free of errors.

Of particular interesting is the case when several triplets are combined ($n_{\text{triplet}} > 1$). For the unregularized MS fit, the weighting bias causes a shift towards negative curvatures (see Figure 6), which increases with n_{triplet} and is quantitatively described by Equation 59. For the regularized MS fit, the curvature bias decreases, according to:.

$$\mathbb{E}[\kappa_{\text{MSreg}}] - \kappa^{\text{true}} = \frac{1}{n_{\text{triplet}}} \frac{\sigma^2_{\kappa_{\text{MSreg}}}}{\kappa^{\text{true}}}. \tag{65}$$

Note that already for $n_{\text{triplet}} = 2$, the (positive) bias of the regularized MS fit is smaller than the (negative) bias of the unregularized MS fit.

As demonstrated for the discussed example, both the MS normalization bias and the weighting bias can significantly deteriorate the curvature measurement if the unregularized MS fit is used. Therefore, preference should be given to the regularized fit if MS uncertainties dominate, since the unregularized MS fit requires an update to reduce the fitting bias.

6. Calculation of Triplet Parameters

The triplet parameters are the input for the global and local triplet fit (Section 3 and Section 4); they are detector-specific and depend on the tracker geometry and the magnetic field. In this section, the four fundamental triplet parameters ($\tilde{\Phi}$, $\tilde{\Theta}$, ρ_ϕ and ρ_θ) are calculated for the most commonly used detector design, which features tracking planes within a uniform solenoidal field (Section 6.1). In section Section 6.2, the case of zero magnetic field is discussed and formulas for measuring the particle momentum just through MS are given.

A gap spectrometer dipole as well as an algorithm for determining the triplet parameters for *any* (inhomogeneous) magnetic field, are discussed in appendices (Appendix E and Appendix F).

6.1. Uniform Magnetic Field

A sketch of a hit triplet in a uniform magnetic field is shown in Figure 7. The z-axis of the spherical coordinate system is aligned with the magnetic field direction, and the x-y plane is the bending plane. In this plane, the line connecting hit 0 and 1 (hit 1 and 2) defines the azimuthal chord angle φ_{01} (φ_{12}), according to:

$$\varphi_{01} := \sphericalangle_\varphi(\vec{x}_1 - \vec{x}_0), \qquad \varphi_{12} := \sphericalangle_\varphi(\vec{x}_2 - \vec{x}_1). \tag{66}$$

The polar angles, θ_{01} and θ_{12}, are defined in the longitudinal s-z plane as:

$$\theta_{01} := \operatorname{acot}\left(\frac{z_{01}}{s_{01}}\right), \qquad \theta_{12} := \operatorname{acot}\left(\frac{z_{12}}{s_{12}}\right), \tag{67}$$

with s_{01} and s_{12} being the transverse arc lengths of the first and second triplet segment, respectively. The corresponding bending angles, Φ_{01} and Φ_{12}, are related to the transverse arc lengths via

$$\Phi_{01} := \frac{s_{01}}{R_{01}} = s_{01}\,\widehat{\kappa_{\perp_{01}}}, \qquad \Phi_{12} := \frac{s_{12}}{R_{12}} = s_{12}\,\widehat{\kappa_{\perp_{12}}}, \tag{68}$$

with $\widehat{\kappa_{\perp_{01}}} = \kappa/\sin(\theta_{01})$ and $\widehat{\kappa_{\perp_{12}}} = \kappa/\sin(\theta_{12})$ being the transverse curvatures of the two segments[13].

[13] Here and in the following, arcs indicate segment curvatures, which always have two indices indicating the connected hits.

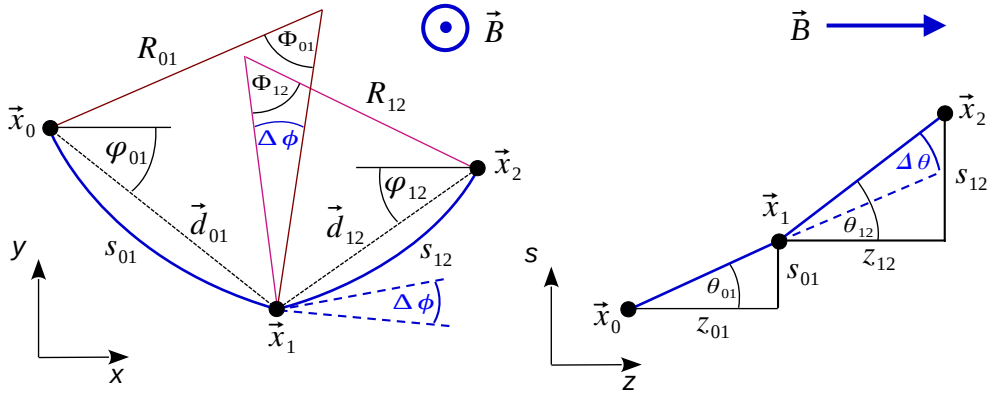

Figure 7: Hit triplet in a uniform magnetic field in the x-y bending plane (*left*) and the s-z non-bending plane (*right*). Hit positions are given by the three points $\vec{x}_0$, $\vec{x}_1$ and $\vec{x}_2$. R_{01} and R_{12} are the transverse bending radii before and after the middle layer. s_{01} and s_{12} denote the transverse arc lengths and Φ_{01} and Φ_{12} the corresponding bending angles. $\vec{d}_{01}$ and $\vec{d}_{12}$ denote the transverse distance vectors between hits in the transverse plane and φ_{01} and φ_{12} are the corresponding azimuthal angles. $\Delta\phi$ is the kink angle in the bending plane. In the non-bending plane, z_{01} and z_{12} define the longitudinal distances between adjacent hits, θ_{01} and θ_{12} the corresponding polar angles and $\Delta\theta$ is the kink angle. Modified from Ref.[7].

With above definitions, the kink angles in the bending and non-bending plane are given by[14]:

$$\Delta\phi = (\varphi_{12} - \varphi_{01}) - \frac{\Phi_{01} + \Phi_{12}}{2} \quad , \tag{69}$$

$$\Delta\theta = \theta_{12} - \theta_{01} \quad . \tag{70}$$

In a uniform magnetic field, the bending angles $\Phi_{kk'}$ and polar angles $\theta_{kk'}$ fulfill the following relations [7]:

$$\sin^2\frac{\Phi_{kk'}}{2} = \frac{1}{4}\kappa^2 d_{kk'}^2 + \kappa^2 z_{kk'}^2 \frac{\sin^2(\Phi_{kk'}/2)}{\Phi_{kk'}^2}, \tag{71}$$

$$\sin\theta_{kk'} = \frac{1}{2}\kappa\, d_{kk'}\, \mathrm{cosec}\left(\frac{\kappa\, z_{kk'}}{2\cos\theta_{kk'}}\right), \tag{72}$$

where k and k' denote two consecutive hits that delimit a segment.

Above equations are transcendent and have multiple solutions, in general. For the hit triplets considered here, only the solution with the smallest bending angle is relevant. Instead of solving the equations above numerically, Equation 71 and Equation 72 are solved with the linearization ansatz introduced in Section 2.1.

For the linearization, the triplet trajectory with $\Delta\phi = 0$ (no kink in the bending plane) is chosen as the reference and will be referred to as the *circle solution* and denoted by the superscript "C" hereafter. The circle solution serves as a suitable reference for linearization, provided that the MS angles are not too large. The transverse curvature of the circle solution, $\kappa_\perp^{\mathrm{C}}$, is readily obtained from the three triplet hit positions 0, 1, 2:

$$\kappa_\perp^{\mathrm{C}} = \frac{2\,\sin(\varphi_{12} - \varphi_{01})}{d_{02}} \tag{73}$$

$$= 2\,\frac{[(\vec{x}_1 - \vec{x}_0)\times(\vec{x}_2 - \vec{x}_1)]_z}{d_{01}\, d_{12}\, d_{02}}. \tag{74}$$

Here, $d_{kk'} := ||(\vec{x}_{k_\perp} - \vec{x}_{k'_\perp})||$ are the hit distances in the transverse plane. For the circle solution, the bending and polar angles are given by:

$$\Phi_{kk'}^{\mathrm{C}} := 2\arcsin\left(\frac{d_{kk'}\,\kappa_\perp^{\mathrm{C}}}{2}\right), \tag{75}$$

$$\cot\theta_{kk'}^{\mathrm{C}} := \frac{z_{kk'}}{d_{kk'}}\frac{\sin(\Phi_{kk'}^{\mathrm{C}}/2)}{\Phi_{kk'}^{\mathrm{C}}/2} = \frac{z_{kk'}\,\kappa_\perp^{\mathrm{C}}}{\Phi_{kk'}^{\mathrm{C}}}, \tag{76}$$

with indices $kk' = 01$ for the first, and $kk' = 12$ for the second segment.

By using the linearization ansatz of Equation 8 and Equation 9, the four fundamental triplet parameters are eventually obtained:

$$\tilde{\Phi} = \frac{1}{2}(\Phi_{01}^{\mathrm{C}}\, n_{01}^{\mathrm{C}} + \Phi_{12}^{\mathrm{C}}\, n_{12}^{\mathrm{C}}), \tag{77}$$

$$\tilde{\Theta} = \theta_{12}^{\mathrm{C}} - \theta_{01}^{\mathrm{C}} + (1 - n_{12}^{\mathrm{C}})\cot\theta_{12}^{\mathrm{C}} - (1 - n_{01}^{\mathrm{C}})\cot\theta_{01}^{\mathrm{C}}, \tag{78}$$

$$\rho_\phi = -\frac{1}{2\,\kappa_\perp^{\mathrm{C}}}\left(\frac{\Phi_{01}^{\mathrm{C}}\, n_{01}^{\mathrm{C}}}{\sin\theta_{01}^{\mathrm{C}}} + \frac{\Phi_{12}^{\mathrm{C}}\, n_{12}^{\mathrm{C}}}{\sin\theta_{12}^{\mathrm{C}}}\right), \tag{79}$$

$$\rho_\theta = \frac{1}{\kappa_\perp^{\mathrm{C}}}\left((1 - n_{01}^{\mathrm{C}})\frac{\cot\theta_{01}^{\mathrm{C}}}{\sin\theta_{01}^{\mathrm{C}}} - (1 - n_{12}^{\mathrm{C}})\frac{\cot\theta_{12}^{\mathrm{C}}}{\sin\theta_{12}^{\mathrm{C}}}\right). \tag{80}$$

The fundamental triplet parameters depend on two index parameters, n_{01}^{C} and n_{12}^{C}, which were first introduced in

[14] Note that different symbols are used for denoting azimuthal angles: φ is used to describe relative hit positions, ϕ is used to describe the track direction, and Φ is used for bending angles.

Ref.[7] and read[15]:

$$n^{\mathrm{C}}_{kk'} \;=\; \left(\frac{\Phi^{\mathrm{C}}_{kk'}}{2} \cot \frac{\Phi^{\mathrm{C}}_{kk'}}{2} \;\sin^2 \theta^{\mathrm{C}}_{kk'} \;+\; \cos^2 \theta^{\mathrm{C}}_{kk'} \right)^{-1}. \quad (81)$$

Note that the index parameters might become singular for recurling tracks, i.e., $|\Phi^{\mathrm{C}}_{kk'}| \geq \pi$. In that case, the corresponding track segment provides an excellent momentum resolution as MS uncertainties vanish in first order [7].

6.1.1. Small Bending Limit

In the limit of small bending angles, $\Phi_{kk'} \to 0$ (e.g. high momentum tracks) the index parameters approach unity, $n^{\mathrm{C}}_{kk'} \to 1$. The fundamental triplet parameters then simplify to:

$$\lim_{\kappa \to 0} \tilde{\Phi} \;=\; \varphi_{12} - \varphi_{01}, \quad (82)$$

$$\lim_{\kappa \to 0} \tilde{\Theta} \;=\; \theta_2 - \theta_1, \quad (83)$$

$$\lim_{\kappa \to 0} \rho_\phi \;=\; -\frac{1}{2}\sqrt{d_{02}^2 + z_{02}^2} \;=\; -\frac{1}{2}||\vec{x}_2 - \vec{x}_0||, \quad (84)$$

$$\lim_{\kappa \to 0} \rho_\theta \;=\; 0. \quad (85)$$

In this limit, the parameters $\tilde{\Theta}$ and $\tilde{\Phi}$ become the triplet kink angles, the ρ_ϕ parameter becomes half the negative chord length of the line connecting the first and third hit, and the ρ_θ parameter vanishes. All fundamental triplet parameters are very simple functions of the triplet geometry in this limit.

6.2. Triplets in Zero Magnetic Field

In the case of zero magnetic field, the triplet trajectory is described by two straight lines with a kink. Although the momentum cannot be measured via the Lorentz force (both triplet ρ-parameters are zero), the amount of MS at the middle tracking layer can be used as an indirect measure of the momentum. The compatibility of the kink angles with MS theory can be tested using the relation:

$$\chi^2_{\mathrm{MS}(B=0)} \;=\; \boldsymbol{\Psi}^\top \boldsymbol{D}_{\mathrm{MS}}(p)\, \boldsymbol{\Psi}. \quad (86)$$

Here hit position errors are neglected for the sake of simplicity. Because of the momentum dependence of the MS errors: $\sigma_{\mathrm{MS}} \propto 1/p$, the right side of Equation 86 can be rescaled:

$$\chi^2_{\mathrm{MS}(B=0)} \;=\; \frac{p^2}{p_0^2}\, (\boldsymbol{\Psi}^\top \boldsymbol{D}_{\mathrm{MS}}(p_0)\, \boldsymbol{\Psi}), \quad (87)$$

where p_0 is a reference momentum that can be freely chosen. Minimizing above equation is not a promising strategy as this would result in $p = 0$, an unphysical solution. A better approach is to "calibrate" the momentum such that the χ^2-value per degree of freedom is 1. This method works reliably for a large number of triplets (hits).

[15] The index parameters were called α_1 and α_2 in [7].

For each triplet, the momentum is the only degree of freedom. After summing over all triplets, the expected mean value of the χ^2 distribution is $\mathbb{E}[\chi^2] = n_{\mathrm{triplet}}$ and the expected variance is $\mathrm{Var}[\chi^2] = 2n_{\mathrm{triplet}}$. The best estimate for a momentum estimation is therefore given by the condition:

$$\chi^2_{\mathrm{MS}(B=0)} \;\stackrel{!}{=}\; n_{\mathrm{triplet}}, \quad (88)$$

resulting in:

$$p_{\mathrm{MS}(B=0)} \;=\; p_0 \sqrt{\frac{n_{\mathrm{triplet}}}{\boldsymbol{\Psi}^\top \boldsymbol{D}_{\mathrm{MS}}(p_0)\, \boldsymbol{\Psi}}}, \quad (89)$$

$$\sigma(p)^2_{\mathrm{MS}(B=0)} \;=\; p_0^2\, \frac{2\, n_{\mathrm{triplet}}}{\boldsymbol{\Psi}^\top \boldsymbol{D}_{\mathrm{MS}}(p_0)\, \boldsymbol{\Psi}}. \quad (90)$$

Both equations can be combined to:

$$\sigma(p)^2_{\mathrm{MS}(B=0)} \;=\; \frac{2\, p^2_{\mathrm{MS}(B=0)}}{n_{\mathrm{triplet}}}. \quad (91)$$

As expected, the relative momentum resolution $\sigma(p)/p$ improves with $1/\sqrt{n_{\mathrm{triplet}}}$.

In the presence of hit position errors, the same method can be used by making the following replacement (see also Equation 27):

$$\boldsymbol{D}_{\mathrm{MS}}(p_0)^{-1} \to\; \boldsymbol{K}^{-1} \;= \boldsymbol{D}_{\mathrm{MS}}(p_0)^{-1} \;+\; \frac{p^2}{p_0^2}\, \vec{\boldsymbol{H}}\, \vec{\boldsymbol{D}}^{-1}_{\mathrm{hit}}\, \vec{\boldsymbol{H}}^\top \quad (92)$$

However, as the momentum determines the relative weight between MS and hit position errors, the solution needs to be determined iteratively.

Above method can be used for time projection chambers or spectrometers, where trackers are located outside the magnetic field region, like the LHCb experiment [15].

7. Energy Loss Correction

Any tracking detector causes energy losses of particles through ionization. For electrons and positrons, also Bremsstrahlung has to be considered. The expected energy loss depends on the effective path length in the material, which is the same as used for the calculation of the MS parameters (Equation 4), and is already known at triplet level.

For thin tracking layers, the corrections to the track fit are typically minor. A simple method to consider small expected energy losses is discussed in Section 7.1 for the local, and in Section 7.2 for the global track fit. For thick tracking layers, however, energy straggling might be significant, requiring a combined fit of the track parameters and the energy losses, which is presented in Section 7.3.

For the sake of simplicity, it is assumed that the particle is highly relativistic, such that the relation $p \sim E$ can be exploited. Furthermore, the calculations below are performed for a uniform magnetic field.

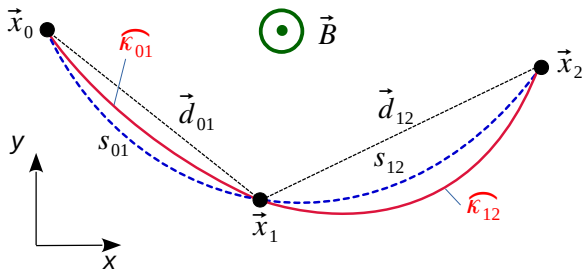

Figure 8: Sketch of a particle trajectory (*red solid* line) with energy loss at the middle triplet layer in a uniform magnetic field. The track curvatures of the segment before and after the energy loss are denoted by $\widehat{\kappa_{01}}$ and $\widehat{\kappa_{12}}$, respectively. For comparison a trajectory without energy loss is shown, which also connects all hits (*blue dashed* line).

7.1. Energy Loss Correction in Local Fit

A hit triplet with hits $k = \{0, 1, 2\}$ is considered. The energy loss at the middle tracking layer Δ_{E_1} changes the 3D curvature, κ, and the trajectory as sketched in Figure 8. Under the assumption of small energy losses, $\Delta_{E_1} \ll qB/\kappa_{01}$, the curvature change is given by:

$$\Delta\kappa_1 = \widehat{\kappa_{12}} - \widehat{\kappa_{01}} = \frac{\Delta_{E_1}}{|\vec{p}|}\,\widehat{\kappa_{01}} \approx \frac{\Delta_{E_1}}{qB}\,\widehat{\kappa_{01}}^2, \tag{93}$$

with $\widehat{\kappa_{01}}$ and $\widehat{\kappa_{12}}$ being the curvature of the first and second segment, respectively, and $\Delta\kappa_1$ being the curvature change at the hit position $k = 1$. The curvatures before and after the energy loss are related to the solution of the triplet fit without energy loss, κ_0, through:

$$\widehat{\kappa_{01}} = \kappa_0 - \frac{s_{12}}{s_{02}}\,\Delta\kappa_1, \tag{94}$$

$$\widehat{\kappa_{12}} = \kappa_0 + \frac{s_{01}}{s_{02}}\,\Delta\kappa_1. \tag{95}$$

Due to the curvature difference between the two segments, the azimuthal track angles are rotated with respect to the $\Delta\kappa_1 = 0$ ($\Delta_{E_1} = 0$) solution. Using the notation from Section 2.1, the rotations in the bending plane at the three hit positions are given by:

$$\Delta\phi_{01} = \phi_{01}^{\Delta_{E_1}} - \phi_{01} = +\frac{s_{01}\,s_{12}}{2\,s_{02}}\,\Delta\kappa_1\,\sin\hat{\theta}, \tag{96}$$

$$\Delta\phi_{10} = \phi_{10}^{\Delta_{E_1}} - \phi_{10} = -\frac{s_{01}\,s_{12}}{2\,s_{02}}\,\Delta\kappa_1\,\sin\hat{\theta}, \tag{97}$$

$$\Delta\phi_{12} = \phi_{12}^{\Delta_{E_1}} - \phi_{12} = -\frac{s_{01}\,s_{12}}{2\,s_{02}}\,\Delta\kappa_1\,\sin\hat{\theta}, \tag{98}$$

$$\Delta\phi_{21} = \phi_{21}^{\Delta_{E_1}} - \phi_{21} = +\frac{s_{01}\,s_{12}}{2\,s_{02}}\,\Delta\kappa_1\,\sin\hat{\theta}, \tag{99}$$

with $\phi_{kk'}^{\Delta_{E_1}}$ and $\phi_{kk'}$ being the azimuthal track angles with and without energy loss at the middle hit position, respectively. Note that the angles ϕ_{10} and ϕ_{12} change in the same way; thus the kink angles and the fit quality of the local fit are not affected by the energy loss, in first order.

7.2. Energy Loss Correction in Global Fit

The expected energy losses at the detection layers are assumed to be known, for example by calculating the expected particle-specific ionization loss from the material distribution. The energy losses are then treated as fixed parameters in the global fit.

The curvature of the segment $\widehat{\kappa_{kk'}}$ can be expressed by the curvature of the first segment, $\widehat{\kappa_{01}}$ and the sum of all curvature changes at the detector layers:

$$\widehat{\kappa_{kk'}} = \widehat{\kappa_{01}} + \sum_{\ell=1}^{k} \Delta\kappa_\ell. \tag{100}$$

For triplet k, the relation between triplet curvature and segment curvature (compare Equation 94) then reads:

$$\kappa_{j=k} = \widehat{\kappa_{kk'}} + \frac{s_{k'k''}}{s_{kk''}}\,\Delta\kappa_{k'}, \tag{101}$$

where the convention $k'' = k' + 1$ and $k' = k + 1$ is used.

Furthermore, an *integrated energy loss* at the hit position k is defined as:

$$I_k := \sum_{\ell=1}^{k} \Delta_{E_\ell}. \tag{102}$$

Using the approximation:

$$\widehat{\kappa_{kk'}} \approx \widehat{\kappa_{01}} + \frac{I_k}{qB}\,\widehat{\kappa_{01}}^2, \tag{103}$$

the triplet curvature at triplet j can be written as:

$$\kappa_{j=k} \approx \widehat{\kappa_{01}} + \frac{I_k^\star}{qB}\,\widehat{\kappa_{01}}^2, \tag{104}$$

Here, $I_j^\star$ denotes an *effective* integrated energy loss, defined by:

$$I_k^\star = I_k + \frac{s_{k'k''}}{s_{kk''}}\,\Delta_{E_{k'}}, \tag{105}$$

which takes into account the energy loss inside the triplet j, see Equation 101.

In this global fit, the first segment curvature $\widehat{\kappa_{01}}$ is chosen as fit parameter. In order to avoid higher order terms of $\widehat{\kappa_{01}}$ in the fit, Equation 104 is linearized using the ansatz:

$$\widehat{\kappa_{01}}^2 = \hat{\kappa}_j^2 + 2(\widehat{\kappa_{01}} - \hat{\kappa}_j) + \mathcal{O}\left((\widehat{\kappa_{01}} - \hat{\kappa}_j)^2\right), \tag{106}$$

with $\hat{\kappa}_j$ being the curvature obtained from the local triplet fit without energy loss.

Equation 104 in linearized from then reads:

$$\kappa_j \approx \widehat{\kappa_{01}}\left(1 + \frac{2\,I_j^\star}{qB}\,\hat{\kappa}_j\right) - \frac{I_j^\star}{qB}\,\hat{\kappa}_j^2\,. \tag{107}$$

By comparing Equation 107 with the linearization ansatz in Equation 17 and Equation 18, one sees that the energy loss inside a triplet corresponds to a change of the triplet

parameters. The linear relationship between κ_j and $\widehat{\kappa_{01}}$ enables the use of the global track fit formulas presented in Section 3 to include energy losses, by making the following substitutions:

$$\tilde{\Theta}_j \;\rightarrow\; \tilde{\Theta}'_j = \tilde{\Theta}_j \;-\; \rho_{\theta,j}\,\frac{I^\star_j}{qB}\,\hat{\kappa}^2_j, \tag{108}$$

$$\tilde{\Phi}_j \;\rightarrow\; \tilde{\Phi}'_j = \tilde{\Phi}_j \;-\; \rho_{\phi,j}\,\frac{I^\star_j}{qB}\,\hat{\kappa}^2_j, \tag{109}$$

$$\rho_{\theta,j} \;\rightarrow\; \rho'_{\theta,j} = \rho_{\theta,j}\left(1 \;+\; \frac{2\,I^\star_j}{qB}\,\hat{\kappa}_j\right), \tag{110}$$

$$\rho_{\phi,j} \;\rightarrow\; \rho'_{\phi,j} = \rho_{\phi,j}\left(1 \;+\; \frac{2\,I^\star_j}{qB}\,\hat{\kappa}_j\right). \tag{111}$$

With above re-interpretation of the fundamental triplet parameters, energy corrections can easily be included in the global triplet track fit[16].

7.3. Combined Track and Energy Loss Fit

For thick tracking detectors, energy straggling might be significant, motivating to include energy losses in the tracking layers as additional fit parameters. Energy losses have usually non-Gaussian tails. However, for the sake of simplicity, a normal distribution is used to derive the fit formulas.

A difficulty arises from the quadratic curvature dependence of the curvature shifts (see e.g. Equation 93) that creates non-linearities in the fit[17]. This problem can be tackled either by using the linearization ansatz from the previous section (Equation 108 to 111) or by re-iterating the fit. In order not to add too much complexity to the discussion, it is assumed that the track curvature (momentum) is known well enough, either from the local triplets or a previous global fit, such that the curvature shifts can be approximated by:

$$\kappa_j - \widehat{\kappa_{01}} \;\approx\; \frac{I^\star_j}{qB}\,\kappa^2_{\mathrm{pre}} \quad , \tag{112}$$

with κ_{pre} being the curvature obtained pre-fit.

If hit position errors are neglected, the fit function reads in matrix representation:

$$\begin{aligned}\chi^2(\widehat{\kappa_{01}},\,\boldsymbol{\varepsilon}) \;&=\; \boldsymbol{\varepsilon}^\top \boldsymbol{D}_{\mathrm{loss}}\,\boldsymbol{\varepsilon} \;+ \\ &\left(\boldsymbol{\Psi} + \boldsymbol{\rho}\,\widehat{\kappa_{01}} - \boldsymbol{R}\,\boldsymbol{\Delta}_E\right)^\top \boldsymbol{D}_{\mathrm{MS}}\,\left(\boldsymbol{\Psi} + \boldsymbol{\rho}\,\widehat{\kappa_{01}} - \boldsymbol{R}\,\boldsymbol{\Delta}_E\right),\end{aligned} \tag{113}$$

with $\widehat{\kappa_{01}}$ being the fit parameter describing the curvature of the first track segment, $\boldsymbol{\Delta}_E$ being a vector describing the energy losses for each tracking layer, $\boldsymbol{\varepsilon}$ being a vector (fit parameter) describing the difference between the fitted energy losses and the expected energy losses, according to $\boldsymbol{\varepsilon} := \boldsymbol{\Delta}_E - \boldsymbol{\Delta}^{\mathrm{exp}}_E$, and $\boldsymbol{D}_{\mathrm{loss}}$ being the energy loss precision matrix (inverse covariance matrix).

The relation between energy losses and kink angle shifts is described by the matrix $\boldsymbol{R}$, which is of size $2\,n_{\mathrm{triplet}} \times n_{\mathrm{triplet}}$, and given by:

$$\boldsymbol{R} \;=\; \frac{\kappa^2_{\mathrm{pre}}}{q\,B}\begin{pmatrix}\mathbf{diag}(\boldsymbol{\rho}_\theta)\;\boldsymbol{\Sigma}\\ \mathbf{diag}(\boldsymbol{\rho}_\phi)\;\boldsymbol{\Sigma}\end{pmatrix}. \tag{114}$$

$\boldsymbol{\Sigma}$ is a quadratic *integration matrix*, which sums up all energy losses before the respective tracking layer:

$$(\boldsymbol{\Sigma})_{jj'} \;=\; \begin{cases} 1 & \text{if} \quad j > j' \\ \frac{s_{j,j+1}}{s_{j-1,j+1}} & \text{if} \quad j = j' \\ 0 & \text{if} \quad j < j' \end{cases}.$$

Note that the index j runs over all triplets and that the energy loss in the very first tracking layer ($k = 0$) and the last tracking layer ($k = n_{\mathrm{hit}} - 1$) are not accounted for in the fit.

The minimization of Equation 113 gives the result:

$$\kappa_{\mathrm{loss}} \;=\; -\frac{\boldsymbol{\rho}^\top \boldsymbol{K}_{\mathrm{loss}}\,\boldsymbol{\Psi}_{\mathrm{loss}}}{\boldsymbol{\rho}^\top \boldsymbol{K}_{\mathrm{loss}}\,\boldsymbol{\rho}}, \tag{115}$$

$$\sigma^2_{\kappa_{\mathrm{loss}}} \;=\; \frac{1}{\boldsymbol{\rho}^\top \boldsymbol{K}_{\mathrm{loss}}\,\boldsymbol{\rho}}, \tag{116}$$

with $\boldsymbol{K}_{\mathrm{loss}}$ being the triplet precision matrix for the energy loss fit, defined as:

$$\boldsymbol{K}^{-1}_{\mathrm{loss}} \;=\; \boldsymbol{D}^{-1}_{\mathrm{MS}} \;+\; \boldsymbol{R}\,\boldsymbol{D}^{-1}_{\mathrm{loss}}\,\boldsymbol{R}^\top, \tag{117}$$

and $\boldsymbol{\Psi}_{\mathrm{loss}}$ being a modified kink angle vector, which includes energy loss effects:

$$\boldsymbol{\Psi}_{\mathrm{loss}} \;=\; \boldsymbol{\Psi} \;+\; \boldsymbol{R}\,\boldsymbol{\Delta}^{\mathrm{exp}}_E. \tag{118}$$

The fit quality then becomes:

$$\chi^2_{\mathrm{loss}} \;=\; \boldsymbol{\Psi}^\top_{\mathrm{loss}} \boldsymbol{K}_{\boldsymbol{\rho}_{\mathrm{loss}}} \boldsymbol{\Psi}_{\mathrm{loss}}, \tag{119}$$

with

$$\boldsymbol{K}_{\boldsymbol{\rho}_{\mathrm{loss}}} \;=\; \left(\boldsymbol{K}_{\mathrm{loss}} - \frac{\boldsymbol{K}_{\mathrm{loss}}\,\boldsymbol{\rho}\boldsymbol{\rho}^\top \boldsymbol{K}_{\mathrm{loss}}}{\boldsymbol{\rho}^\top \boldsymbol{K}_{\mathrm{loss}}\,\boldsymbol{\rho}}\right). \tag{120}$$

Above results are identical to the general fit that includes hit position errors when the hit residuals are replaced by the energy losses, and the matrix $\vec{\boldsymbol{H}}$ is replaced by the matrix $\boldsymbol{R}$. Accordingly, one obtains for the fitted energy loss vector:

$$\boldsymbol{\Delta}_E \;=\; \boldsymbol{\Delta}^{\mathrm{exp}}_E \;+\; \boldsymbol{D}^{-1}_{\mathrm{loss}}\,\boldsymbol{R}^\top\;\boldsymbol{K}_{\boldsymbol{\rho}_{\mathrm{loss}}}\,\boldsymbol{\Psi}_{\mathrm{loss}}, \tag{121}$$

and for the corresponding covariance matrix:

$$\mathbf{Cov}_{\boldsymbol{\varepsilon}} \;=\; \boldsymbol{D}^{-1}_{\mathrm{loss}} - \;\boldsymbol{D}^{-1}_{\mathrm{loss}}\,\boldsymbol{R}^\top \boldsymbol{K}_{\boldsymbol{\rho}_{\mathrm{loss}}}\,\boldsymbol{R}\,\boldsymbol{D}^{-1}_{\mathrm{loss}}. \tag{122}$$

It is straightforward to also include hit errors in the fit.

[16] It is important to note that the locally fitted curvatures $\hat{\kappa}_j$ should only be used in above equations if they are reliably measured by the triplets. An alternative strategy is to repeat the global fit, after neglecting the energy loss in the first step, and using the curvature result of the first fit as reference.

[17] This problem does not arise if the 3D radius $R_{3\mathrm{D}} = \kappa$ is chosen as fit parameter, as done in Ref.[7].

8. Triplet Fit Parallelization and Computational Effort

The approach of splitting a set of hits into triplets primarily aims to enhance the parallelizability of track fitting and track reconstruction programs, which is especially important for high-rate experiments where the track reconstruction is rate-limited. The GTTF has three steps: the calculation of the triplet parameters, the local triplet fit (optional filtering step), and the global triplet track fit. The possible savings in computational effort through parallelization for each step are discussed below.

Triplet Parameters and Hit Gradients. Two main cases can be distinguished. In the most general case (e.g. inhomogeneous magnetic field) the triplet parameters need to be derived from at least 2×4 track extrapolations per triplet (see Appendix F for details), which are *independent* and can be parallelized.

In case that an analytical solution for the triplet parameters exists (e.g. uniform magnetic field, see Section 6.1), computationally expensive track extrapolations are not required. The determination of the up to 3×3 hit gradients then only involves simple geometrical (re-)calculations. If MS errors dominate, the calculation of the hit gradients is not required. Since the triplet parameters of all triplets are independent, the triplet parameter calculation can be fully parallelized. Note that in track reconstruction tasks, each triplet parameter needs to be calculated only once, even if it belongs to several track candidates. This step can significantly profit from parallel hardware architectures like GPUs.

Local Triplet Fit as Filtering Step. Hit triplets are often used as seeds in track reconstruction; an early filtering step can be very useful to reduce hit combinatorics and speed up processing time. The filtering step consists of calculating the local triplet fit quality (Equation 48) and applying a quality cut. Only for accepted triplets, the momentum and its error need to be calculated to enable checking the consistency of the momentum with other triplets. This step can also be fully parallelized.

Global Triplet Track Fit. In the general case, where hit position errors cannot be neglected, the inversion of the triplet covariance matrix, $\boldsymbol{K}^{-1}$, is the most time-consuming step, if the number of tracking layers is large. The limited ability to accelerate this step highlights the importance of the local triplet fit as an early filtering step. The situation is different in case of dominant MS errors, where $\boldsymbol{K}^{-1}$ is diagonal, and full parallelization is possible. The global fit quality, the track curvature, and its error can then be easily calculated from simple sums, see Equations 32 to 34. The computational effort is then marginal and the required calculations can be efficiently implemented on parallel hardware architectures like GPUs.

Modern silicon pixel detectors offer superb spatial resolution; and high-momentum particles – for which hit position uncertainties dominate – are relatively rare in hadron collider experiments. As a result, the GTTF can be implemented in an almost fully parallelized manner. An interesting aspect is the collection of filtered triplets and their subsequent combination into track candidates, ultimately forming a graph whose size depends on the purity of the filtered triplets. Resolving triplet (hit) ambiguities is actually equivalent to disconnecting the graphs [16], a task that can be efficiently tackled by GNNs [17] and cellular automata [18]. The latter has been studied in a recent work in combination with the GTTF [19].

9. Tracking Regimes

The GTTF provides closed-form expressions for the track parameters and the covariance matrix, enabling an easy identification of the dominant sources of the track parameter uncertainties, and an assessment of the measurement accuracy of the triplet. By using a classification scheme, which is described below, different *tracking regimes* can be defined. For the classification, two new quantities are introduced: the *tracking scale parameter* and the *curvature significance parameter*. Both parameters provide important input for accelerating track reconstruction, see discussion in Section 8, and can also aid in optimizing tracking detector designs.

9.1. The Tracking Scale Parameter

The track parameter uncertainties are determined by the triplet precision matrix $\boldsymbol{K}$ (Equation 27), which depends on the triplet uncertainties ${\Gamma_{\phi\phi}}^{\star}$ and ${\Gamma_{\theta\theta}}^{\star}$ (Equation 43 and Equation 44). These parameters combine hit position and MS errors.

For each triplet, the relative fraction of the hit position errors (variance) can be used to define two tracking scale parameters:

$$\mu_\phi^2 := \frac{\Gamma_{\phi\phi}}{{\Gamma_{\phi\phi}}^{\star}}, \qquad \mu_\theta^2 := \frac{\Gamma_{\theta\theta}}{{\Gamma_{\theta\theta}}^{\star}}. \tag{123}$$

The values of μ_ϕ and μ_θ are in the range from 0 for dominant MS errors (low momentum regime) to 1 for dominant hit position errors (high momentum regime).

The tracking scale parameters are of practical relevance for track fitting. In the case that the tracking scale parameters are small ($\mu_{\phi,\theta} \lesssim 0.15$), the fast MS fit can be used[18], whereas in all other cases the general fit should be used, which requires the inversion of the triplet covariance matrix $\boldsymbol{K}^{-1}$. The tracking scale parameter thus defines a criterion for determining whether the track fit can be accelerated.

[18] For $\rho_\phi^2 \gg \rho_\theta^2$ (small bending), only the tracking scale parameter μ_ϕ is relevant.

9.2. The Curvature Significance Parameter

The curvature significance parameter, ξ, is defined by the ratio of the curvature over its error:

$$\xi^2 := \frac{\kappa^2}{\sigma^2_\kappa}, \tag{124}$$

and quantifies how precisely the track curvature is measured. The parameter allows to distinguish between the strong bending regime, $\xi^2 \gg 1$, where a precise momentum measurement is possible, and the weak bending regime, $\xi^2 \approx 0$, where no momentum measurement is possible.

9.2.1. Dominant MS Uncertainties ($\mu^2 = 0$)

For a tracking detector in a uniform magnetic field, the following relation is obtained if MS uncertainties dominate:

$$\xi^2_{\mathrm{MS}} = \frac{{\kappa_{\mathrm{MS}}}^2}{\sigma^2_{\kappa_{\mathrm{MS}}}} \approx \frac{\tilde{\Phi}^2}{\sigma^2_{\phi_{\mathrm{MS}}}}. \tag{125}$$

In the small bending limit (Section 6.1.1), the last expression can be rewritten as:

$$\xi^2_{\mathrm{MS}} \approx \frac{a^2}{4\, b^2_{\mathrm{MS}}}, \tag{126}$$

with a being the length of the triplet in Euclidean space (compare Equation 84) and b_{MS} being the MS parameter (Equation 3). ξ_{MS} is independent of the particle momentum and characterizes the tracking detector quality for MS dominance. The requirement to measure the track curvature with 3σ significance corresponds to the condition $\frac{a}{2\, b_{\mathrm{MS}}} \gtrsim 3$, a criterion first formulated in Ref.[7].

It should be remarked that ξ_{MS} is also related to the fitting bias discussed in Section 5 and that for $\xi_{\mathrm{MS}} < 10$ significant biases ($> 1\,\%$) of the momentum (curvature) can occur.

9.2.2. General case

For non-negligible hit position errors (general case), the curvature significance parameter (Equation 124) can be generalized by including the tracking scale parameter (Equation 123):

$$\xi = \xi_{\mathrm{MS}} \cdot \sqrt{1 - \mu^2_\phi}. \tag{127}$$

As expected, the curvature significance decreases as the contribution of hit position errors increases (larger μ_ϕ), which corresponds to higher track momenta.

9.3. Examples of Tracking Regimes in Pixel Detectors

For illustration, the μ_ϕ and ξ parameters are calculated for several pixel detectors: the upgraded ALICE experiment [20, 21], the upgraded ATLAS experiment [22], and the Mu3e experiment [9]. These detectors are here selected as they cover a wide range of particle momenta from $\mathcal{O}(10\,\mathrm{MeV/c})$ at the Mu3e experiment up to $\mathcal{O}(1000\,\mathrm{GeV/c})$

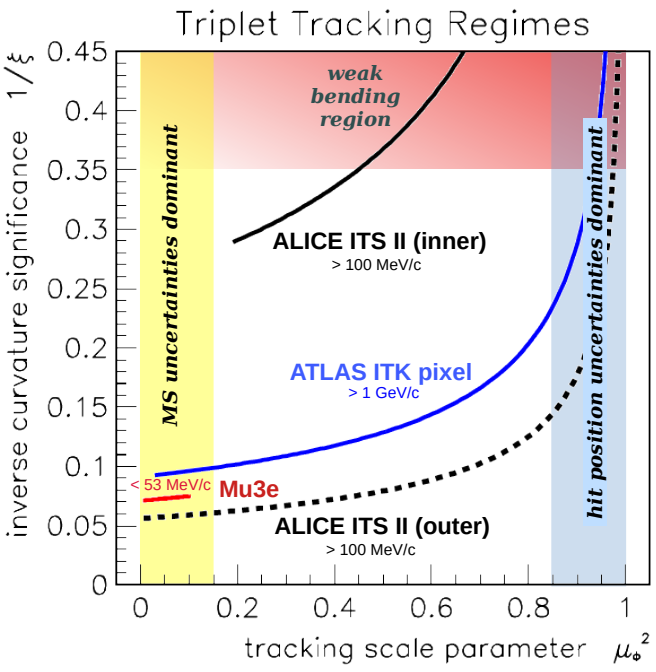

Figure 9: Parameter space spanned by the normalized MS parameter scale ξ and the tracking scale parameter μ_ϕ for various pixel tracking detectors: ALICE ITS II inner and outer pixel tracking detector (*black*), ATLAS ITK (*blue*) and Mu3e (*red*). The curves cover the momentum range $0.1 - 100\,\mathrm{GeV/c}$ for ALICE, $1 - 1000\,\mathrm{GeV/c}$ for ATLAS, and 10 - 53 MeV/c for Mu3e.

at the ATLAS experiment. Based on the detector description in the respective technical design reports, the tracking regime parameters are derived from hit triplets in the central tracking regions. The μ_ϕ - $1/\xi$ parameter space for the above mentioned pixel trackers is shown in Figure 9, and discussed below.

ALICE Inner Tracking System (ITS II). The ITS II detector [20, 21] is in operation since 2024. It consists of three inner pixel layers with a radiation length of $X/X_0 = 0.35\,\%$ and four outer pixel layers with a radiation length of $X/X_0 = 1\,\%$. The distance between the inner pixel layers is only $\sim 10\,\mathrm{mm}$, which, together with the relatively moderate field of $B = 0.5\,\mathrm{T}$, results in a low curvature significance of $\xi_{\mathrm{MS}} \sim 3.8$, despite the small amount of tracking material. With the Inner ITS II detector alone, a 3σ measurement of track curvatures is only possible for very low momenta ($p \lesssim 150\,\mathrm{MeV/c}$). However, it should be mentioned that the main purpose of the Inner ITS II detector is vertexing and not the momentum measurement.

The situation is different for the Outer ITS II detector, where the tracking layers are separated by about 80 mm. The curvature significance for low-momentum tracks is $\xi_{\mathrm{MS}} \sim 18$ and a 3σ measurement of track curvatures is possible for a single triplet up to $15\,\mathrm{GeV/c}$, thanks to the high resolution of the ALPIDE sensors [23].

ATLAS Inner TracKer (ITK). The ITK tracking system[22] of the high luminosity upgraded ATLAS experiment was

optimized to reconstruct charged particles at very high particle rates, with up to 200 collisions per bunch crossing. Similar to the Inner ITS II detector, the main purpose of the ATLAS pixel detector is to reconstruct primary and secondary vertices. Due to the high radiation length of about $X/X_0 = 1.5\,\%$ per tracking layer in the central region, a curvature significance of $\xi_{\text{MS}} \sim 11$ is only reached for very low-momentum tracks. A 3σ measurement of the curvature is possible for a single triplet up to $20\,\text{GeV/c}$, thanks to the high field of $B = 2\,\text{T}$.

Mu3e Pixel Tracker. The Mu3e pixel detector [9] has an ultra-light pixel detector design with a radiation length of about $X/X_0 = 0.11\,\%$ per tracking layer, and was optimized for tracking low-momentum electrons and positrons from muon decays in the momentum range $12 - 53\,\text{MeV/c}$. The tracking scale parameter is $\mu_\phi^2 \leq 0.1$ for all momenta, such that the fast MS track fit can be exploited for all tracks. The curvature significance is about $\xi \sim 14$ in the full momentum range. Note that the Mu3e pixel detector exploits recurling tracks, which provide an about 7 times better momentum resolution, corresponding to $\xi \sim 100$.

The above examples show how the tracking scale parameter μ_ϕ and the curvature significance ξ distinguish different tracking regimes, which would require different implementations to accelerate the GTTF. Furthermore, the curvature significance also defines a metric for the ability to resolve inevitable hit ambiguities in the track reconstruction: triplets with large ξ-values restrict the phase space more than low ξ triplets. For track reconstruction, high ξ triplets are better suited than low ξ triplets as they provide higher precision in track extrapolations and more stringent consistency checks (e.g. consistency of triplet momenta). Consequently, the proposed tracking regime analysis can serve as a valuable tool for track reconstruction optimization.

10. Summary

In this paper a new track fit, the General Triplet Track Fit (GTTF) was presented. The solution of the fit is given in an analytical closed-form. All formulas are based on so-called triplet parameters which contain the detector-specific information such as geometry, detector material and the magnetic field. The fit is generic and takes into account material effects such as MS and energy loss, as well as hit position uncertainties. The triplet representation makes the track fit universal, since the same fitting code can be used for all kind of tracking detectors.

Triplet parameters are derived for various tracking detector configurations. It is shown that in the case of small bending (high momentum tracks), the triplet parameters become simple geometrical constants. For the triplet parameter calculation in a general (inhomogeneous) magnetic field, an algorithm employing track extrapolation is presented. Furthermore, two methods for including energy losses are described: one that treats the expected energy loss as an additional input (suitable for small energy losses), and one that fits the energy loss for each tracking layer (suitable for large energy losses).

The output of the GTTF consists of the particle momentum (3D curvature), all hit residuals, and the full covariance matrix. From this, the state vector of the track, which is needed for track extrapolation (vertexing), can be calculated at any point of the trajectory. Formulas to calculate the state vector and the corresponding covariance matrix are provided in the appendix.

The GTTF can be fully parallelized on triplet level. Due to the high degree of parallelization, the GTTF is ideal for its implementation on parallel hardware architectures such as GPUs. Furthermore, the fit of a single hit triplet is over-constrained, thus making it possible to calculate a fit quality on triplet level and to apply filters. This (optional) filtering step offers the possibility to accelerate track reconstruction at an early stage.

The GTTF provides several options for algorithmic acceleration, the most important being the MS fit, which does not require a computationally expensive matrix inversion, in contrast to the global fit. Two new parameters are introduced, the *tracking scale parameter* and the *curvature significance parameter*, to classify different tracking regimes, for which different track fit approximations and optimizations apply.

An interesting application for the tracking regime-specific track fit acceleration is track reconstruction at hadron colliders. Since most particles produced in hadron interactions are at low momenta and dominated by MS, significant amount of computating time can be saved by performing the fast MS fit. It is recommended to execute the more time-expensive generic fit only if hit position errors cannot be neglected ($\mu_{\phi,\theta} \gtrsim 0.15$). An optimization of the track reconstruction based on the tracking regime concept is of high relevance for real-time applications, in particular in environments with high particle rates. The analysis of tracking regimes can also provide useful information for the design of new tracking detectors.

The analytical closed-form of the GTTF also enables the study of the inherent fitting bias in the MS tracking model. A detailed study of the bias in MS dominated track fit is performed. Mitigation strategies are discussed and a regularized track fit is presented, which reduces track fit biases.

Finally, it is important to note that the GTTF can be easily extended to incorporate geometric alignment parameters, which will be addressed in a follow-up article.

Acknowledgments

The author thanks several group members and colleagues for many useful discussions on this topic and for proofreading: Niklaus Berger, Sebastian Dittmeier, David

Fritz, Tamasi Kar, Alexandr Kozlinskiy, Abhirikshma Nandi, and Christof Sauer.

A. Global Fit for Dominant Hit Position Errors

In the limit of dominant hit position errors, the MS errors can be neglected. According to Equation 27, the precision matrix becomes:

$$\boldsymbol{K} \to \boldsymbol{K}_{\text{hit}} \;:=\; (\vec{\boldsymbol{H}}\vec{\vec{\boldsymbol{D}}}_{\text{hit}}^{-1}\vec{\boldsymbol{H}}^{\top})^{-1}. \tag{A.1}$$

The 3D curvature and its uncertainties are then given by:

$$\kappa_{\text{hit}} \;=\; -\frac{\boldsymbol{\rho}^{\top}\boldsymbol{K}_{\text{hit}}\,\boldsymbol{\Psi}}{\boldsymbol{\rho}^{\top}\boldsymbol{K}_{\text{hit}}\,\boldsymbol{\rho}}, \tag{A.2}$$

$$\sigma^2_{\kappa_{\text{hit}}} \;=\; \frac{1}{\boldsymbol{\rho}^{\top}\boldsymbol{K}_{\text{hit}}\,\boldsymbol{\rho}}. \tag{A.3}$$

Furthermore, the hit positions shifts and the corresponding covariance matrix are given by:

$$\vec{\boldsymbol{\delta}}_{\text{hit}} \;=\; \vec{\vec{\boldsymbol{D}}}_{\text{hit}}^{-1}\vec{\boldsymbol{H}}^{\top}\,\boldsymbol{K}_{\boldsymbol{\rho}\text{hit}}\,\boldsymbol{\Psi}, \tag{A.4}$$

$$\vec{\vec{\mathbf{Cov}}}_{\delta_{\text{hit}}} \;=\; \vec{\vec{\boldsymbol{D}}}_{\text{hit}}^{-1} - \vec{\vec{\boldsymbol{D}}}_{\text{hit}}^{-1}\vec{\boldsymbol{H}}^{\top}\boldsymbol{K}_{\boldsymbol{\rho}\text{hit}}\,\vec{\boldsymbol{H}}\,\vec{\vec{\boldsymbol{D}}}_{\text{hit}}^{-1}. \tag{A.5}$$

Here, $\boldsymbol{K}_{\boldsymbol{\rho}\text{hit}}$ is defined similar to Equation 29:

$$\boldsymbol{K}_{\boldsymbol{\rho}\text{hit}} \;=\; \left(\boldsymbol{K}_{\text{hit}} - \frac{\boldsymbol{K}_{\text{hit}}\,\boldsymbol{\rho}\boldsymbol{\rho}^{\top}\boldsymbol{K}_{\text{hit}}}{\boldsymbol{\rho}^{\top}\boldsymbol{K}_{\text{hit}}\,\boldsymbol{\rho}}\right).$$

Finally, the fit quality is given by:

$$\chi^2_{\text{hit}} \;=\; \boldsymbol{\delta}^{\top}\vec{\vec{\boldsymbol{D}}}_{\text{hit}}\,\boldsymbol{\delta} \tag{A.6}$$

$$\;=\; \boldsymbol{\Psi}^{\top}\boldsymbol{K}_{\boldsymbol{\rho}\text{hit}}\boldsymbol{\Psi}. \tag{A.7}$$

Note that in the first line of Equation A.6 the sums are executed over all hit uncertainty directions whereas in the second line (Equation A.7) the sums run over twice the number of triplets.

B. Regularized Local MS Fit

The formulas for the regularized global MS fit are discussed in Section 5.3. For a single triplet, the fit result is given by:

$$\kappa_{\text{MSreg}} \;=\; -\,\frac{\tilde{\Phi}^2\,\sin^2\hat{\theta} + \tilde{\Theta}^2}{\tilde{\Phi}\,\rho_{\phi}\,\sin^2\hat{\theta} + \tilde{\Theta}\,\rho_{\theta}}, \tag{B.1}$$

$$\sigma_{\kappa_{\text{MSreg}}} \;=\; b_{\text{MS}}\,\frac{(\tilde{\Phi}^2\,\sin^2\hat{\theta} + \tilde{\Theta}^2)^{\frac{3}{2}}}{(\tilde{\Phi}\,\rho_{\phi}\,\sin^2\hat{\theta} + \tilde{\Theta}\,\rho_{\theta})^2}, \tag{B.2}$$

$$\chi^2_{\text{MSreg}} \;=\; \frac{1}{b^2_{\text{MS}}}\,\frac{(\tilde{\Phi}\,\rho_{\theta} - \tilde{\Theta}\,\rho_{\phi})^2}{\tilde{\Phi}^2 + \tilde{\Theta}^2/\sin^2\hat{\theta}}. \tag{B.3}$$

C. Strip Detectors

In this section, the local triplet fit is discussed for a barrel-type strip detector in a uniform magnetic field. In the context of the triplet fit, a detector is defined to be a strip detector if large hit position errors in one detector direction create a significant rotational triplet uncertainty. In the following formulas for the local triplet fit are derived, which include the hit position dependence of the triplet parameters that has been neglected in Section 3 and Section 4. Rotational uncertainties in the global triplet fit are usually negligible if several triplets are combined.

The configuration with strips oriented in axial direction is considered here, which is used in many experiments. Since $\sigma_z \gg \sigma_{\phi}$, such a detector is not able to precisely measure the polar angle. This, however, affects the 3D curvature via the relation $\kappa = \kappa_{\perp}\,\sin\theta$.

With the assumptions $\Gamma_{\theta\theta} \gg \sigma^2_{\text{MS}}$ and $\Gamma_{\theta\theta} \gg \Gamma_{\phi\phi}$, Equation 46 (and the following equations) can be approximated as:

$$\kappa_{z\text{-strip}} \;\approx\; -\frac{\tilde{\Phi}}{\rho_{\phi}} \;+\; \Delta\kappa_{\text{rot}}, \tag{C.1}$$

$$\sigma^2_{\kappa,z\text{-strip}} \;\approx\; \frac{{\Gamma_{\phi\phi}}^{\star}}{\rho^2_{\phi}} \;+\; \Delta\sigma^2_{\kappa,\text{rot}}, \tag{C.2}$$

$$\chi^2_{z\text{-strip}} \;\approx\; \frac{\tilde{\Theta}^2}{\Gamma_{\theta\theta}}, \tag{C.3}$$

where additional correction term are added to account for the rotational uncertainty. They are calculated as:

$$\Delta\kappa_{\text{rot}} \;=\; -\frac{\tilde{\Phi}}{\rho_{\phi}}\,\Delta\theta_{\text{rot}}\cot\hat{\theta}, \tag{C.4}$$

$$\Delta\sigma^2_{\kappa_{\text{rot}}} \;=\; \kappa^2_{z\text{-strip}}\,\sigma^2_{\theta_{\text{rot}}}\,\cot\hat{\theta}, \tag{C.5}$$

and depend on the triplet rotation and its error:

$$\Delta\theta_{\text{rot}} \;=\; \frac{\tilde{\Theta}}{2\Gamma_{\theta\theta}}\left(\vec{\delta}_2\,\vec{h}_{\theta_2} - \vec{\delta}_0\,\vec{h}_{\theta_0}\right), \tag{C.6}$$

$$\sigma^2_{\theta_{\text{rot}}} \;=\; \frac{1}{4}\left(\vec{h}^{\,t}_{\theta_0}\vec{\vec{V}}'\,\vec{h}_{\theta_0} + \vec{h}^{\,t}_{\theta_2}\vec{\vec{V}}'\,\vec{h}_{\theta_2}\right). \tag{C.7}$$

D. Track Parameters and Covariance Matrix

In a broken line fit such as the GTTF, kinks in the trajectory must be taken into in the determination of the track parameters. In the following it is assumed that all detector material in the active tracking region is located at the tracking layers. The position of the kinks thus agrees with the position of the hits. For vertexing (extrapolation to the track origin), the track parameters need to be determined at the first hit ($k = 0$). For track extrapolation in the other direction, the track parameters need to be determined at the last hit ($k = n_{\text{hit}} - 1$). Note that for track extrapolation the material in the first (last) detector layer must be considered as extra scatterer (like any other material, e.g. beam pipes) since this material is not included in the track fit.

For track parameterization, the following representation is used:

$$\bar{t} = (\vec{x}, \kappa, \theta, \phi), \tag{D.1}$$

with the corresponding covariance matrix defined as:

$$\bar{\bar{\mathrm{Cov}}}_t = \begin{pmatrix} \vec{\vec{\mathrm{Cov}}}(\vec{x},\vec{x}) & \mathrm{Cov}(\kappa,\vec{x}) & \mathrm{Cov}(\theta,\vec{x}) & \mathrm{Cov}(\phi,\vec{x}) \\ \mathrm{Cov}(\vec{x},\kappa) & \mathrm{Var}(\kappa) & \mathrm{Cov}(\theta,\kappa) & \mathrm{Cov}(\phi,\kappa) \\ \mathrm{Cov}(\vec{x},\theta) & \mathrm{Cov}(\kappa,\theta) & \mathrm{Var}(\theta) & \mathrm{Cov}(\phi,\theta) \\ \mathrm{Cov}(\vec{x},\phi) & \mathrm{Cov}(\kappa,\phi) & \mathrm{Cov}(\theta,\phi) & \mathrm{Var}(\phi) \end{pmatrix} \tag{D.2}$$

Here and below, the bar $^-$ indicates a vector and the double bar $^=$ a matrix in the six-dimensional track parameter space.

D.1. Track Position and Uncertainties

Be hit k the starting point of the track extrapolation, the track position in global coordinates is obtained from the fitted residuals (Equation 28) via the relation:

$$\vec{x}_{k,\mathrm{fit}} = \vec{x}_k + \vec{\vec{Q}}_k^{\top}\, \vec{\delta}_k, \tag{D.3}$$

with $\vec{\vec{Q}}_k^{\top}$ being the back-rotation from local to global coordinates, see also Equation 10. The corresponding covariance matrix in global coordinates is derived from the local covariance matrix via the transformation:

$$\vec{\vec{\mathrm{Cov}}}(\vec{x}_k,\vec{x}_k) \;=\; (\vec{\vec{\mathbf{Cov}}}_x)_k = \; (\vec{\vec{\boldsymbol{Q}}}^{\top}\, \vec{\vec{\mathbf{Cov}}}_\delta\, \vec{\vec{\boldsymbol{Q}}})_k, \tag{D.4}$$

where $\vec{\vec{\mathbf{Cov}}}_\delta$ is given by:

$$\vec{\vec{\mathbf{Cov}}}_\delta \;=\; \vec{\vec{\boldsymbol{D}}}_{\mathrm{hit}}^{-1} - \vec{\vec{\boldsymbol{D}}}_{\mathrm{hit}}^{-1}\, \vec{\boldsymbol{H}}^{\top}\, \boldsymbol{K}_{\boldsymbol{\rho}}\, \vec{\boldsymbol{H}}\, \vec{\vec{\boldsymbol{D}}}_{\mathrm{hit}}^{-1}. \tag{29}$$

D.2. Track Parameter Representation

The track vector in local coordinate transformation, $\bar{t}_{\mathrm{loc}}$, is defined equivalent to Equation D.1:

$$\bar{t}_{\mathrm{loc}} = (\vec{\delta}, \kappa, \theta, \phi). \tag{D.5}$$

For the transformation to global coordinates a 6×6 matrix is defined:

$$\bar{\bar{G}} := \begin{pmatrix} \vec{\vec{Q}}^{\top} & 0 & 0 & 0 \\ 0 & 1 & 0 & 0 \\ 0 & 0 & 1 & 0 \\ 0 & 0 & 0 & 1 \end{pmatrix}. \tag{D.6}$$

The track parameters and the corresponding error matrix then transform as:

$$\bar{t} = \bar{\bar{G}}^{-1}\, \bar{t}_{\mathrm{loc}} \tag{D.7}$$

$$\bar{\bar{\mathrm{Cov}}}_t = \bar{\bar{G}}\, \bar{\bar{\mathrm{Cov}}}_{t_{\mathrm{loc}}}\, \bar{\bar{G}}^{-1}. \tag{D.8}$$

Note that the curvature and track angles are defined in global coordinates and not transformed.

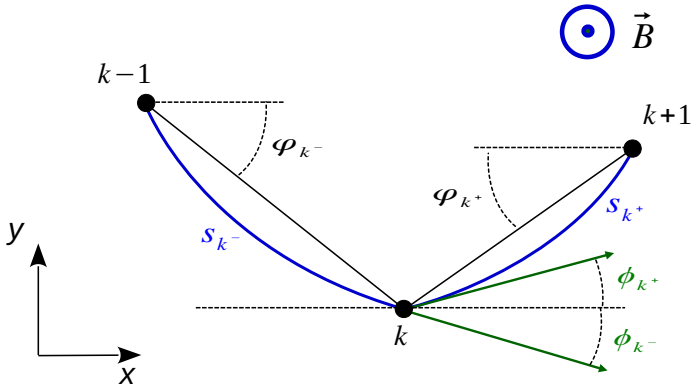

Figure D.10: Azimuthal (*left*) and polar (*right*) track angles at the hit position k using the short-hand notation introduced in Equation D.12 and Equation D.11. In a uniform magnetic field, the arc lengths are related to the bending angles via $s_{k\pm} = \Phi_{k\pm} R_{k\pm}$, with $R_{k\pm}$ being the bending radius.

D.3. Track Curvature

For the general case, the 3D curvature and its variance are given by (see Section 3):

$$\kappa \;=\; -\frac{\boldsymbol{\rho}^{\top}\boldsymbol{K}\boldsymbol{\Psi}}{\boldsymbol{\rho}^{\top}\boldsymbol{K}\boldsymbol{\rho}}, \tag{25}$$

$$\mathrm{Var}(\kappa) \;=\; \frac{1}{\boldsymbol{\rho}^{\top}\boldsymbol{K}\boldsymbol{\rho}}. \tag{26}$$

The correlated error between the fitted curvature and the hit position k is given by:

$$\mathrm{Cov}(\vec{\delta}_k,\kappa) \;=\; (\vec{\mathbf{Cov}}_{\delta/\kappa})_k, \tag{D.9}$$

with

$$\vec{\mathbf{Cov}}_{\delta/\kappa} \;=\; \frac{\vec{\vec{\boldsymbol{D}}}_{\mathrm{hit}}^{-1}\vec{\boldsymbol{H}}^{\top}\boldsymbol{K}\,\boldsymbol{\rho}}{\boldsymbol{\rho}^{\top}\boldsymbol{K}\,\boldsymbol{\rho}}. \tag{D.10}$$

D.4. Track Direction

The determination of the track direction is more evolved since the track direction is position dependent in a magnetic field. For an inhomogeneous magnetic field, the track direction can be determined using the method described in Appendix F.

For a uniform magnetic field (Section 6.1) the polar and azimuthal angles of a trajectory at hit position k are given as follows:

$$\theta_{k^\pm} \;=\; \mathrm{acot}\left[\frac{z_{k^\pm}}{d_{k^\pm}}\,\frac{\sin(\Phi_{k^\pm}/2)}{\Phi_{k^\pm}/2}\right], \tag{D.11}$$

$$\phi_{k^\pm} \;=\; \varphi_{k^\pm} \mp \frac{\Phi_{k^\pm}}{2}, \tag{D.12}$$

where a short-hand notation for the indices is used: $k^\pm =$ "$k, k\pm 1$". The $\pm$ sign refers here to the two solutions

after/before the scattering at tracking layer k, see Figure D.10. Note that for the first (last) hit of a track only a solution with the + (−) sign exists and that $\varphi_{k^\pm}$ is defined by Equation 66. Further note that all parameters in Equation D.11 and Equation D.12 are post-fit.

Curvature Dependence. Both Equation D.11 and Equation D.12 require knowledge of the bending angle $\Phi_{k^\pm}$, which in turn depends on the curvature κ. The GTTF consistently employs the small multiple scattering approximation, which assumes that the triplet trajectory can be linearized around the circle solution in the bending plane (Equation 7).

At segment level, the linearization of the polar and bending angle yields:

$$\theta(\kappa)_{k^\pm} \;=\; \theta^{\mathrm{C}}_{k^\pm} + \tau_{k^\pm} + \kappa\,\widehat{\rho}_{\theta\,k^\pm}, \tag{D.13}$$

$$\Phi(\kappa)_{k^\pm} \;=\; \nu_{k^\pm} \;+\; \kappa\,\widehat{\rho}_{\phi\,k^\pm}, \tag{D.14}$$

where new segment-specific linearization parameters are introduced:

$$\widehat{\rho}_{\theta\,k^\pm} \;:=\; \frac{n^{\mathrm{C}}_{k^\pm} - 1}{\widehat{\kappa}^{\mathrm{C}}_{k^\pm}} \cot\theta^{\mathrm{C}}_{k^\pm}, \tag{D.15}$$

$$\widehat{\rho}_{\phi\,k^\pm} \;:=\; \frac{n^{\mathrm{C}}_{k^\pm}}{\widehat{\kappa}^{\mathrm{C}}_{k^\pm}}\,\Phi^{\mathrm{C}}_{k^\pm}, \tag{D.16}$$

$$\tau_{k^\pm} \;:=\; (1 - n^{\mathrm{C}}_{k^\pm})\cot\theta^{\mathrm{C}}_{k^\pm}, \tag{D.17}$$

$$\nu_{k^\pm} \;:=\; (1 - n^{\mathrm{C}}_{k^\pm})\,\Phi^{\mathrm{C}}_{k^\pm}, \tag{D.18}$$

with $\widehat{\kappa}^{\mathrm{C}}_{k^\pm}$ being segment-wise 3D curvatures, given by:

$$\widehat{\kappa}^{\mathrm{C}}_{k^\pm} \;=\; \kappa^{\mathrm{C}}_{\perp_j}\,\sin\theta^{\mathrm{C}}_{k^\pm} \tag{D.19}$$

As in Section 6.1, the index C always refers to the circle solution.

The triplet index $j \in k-1, k$ indicates which of two possible triplets per segment is chosen to determine the circle solution. Note that the $\widehat{\ }$ is used here and below to distinguish the segment-wise defined $\widehat{\rho}$ parameters (Equation D.15 and Equation D.16) from the triplet-wise defined ρ parameters (Equation 8 and Equation 9). Further note that the segment-wise $\widehat{\rho}$ parameters are related to the triplet ρ parameters (see also Section 6.1) via $\rho_\phi = -\frac{1}{2}(\widehat{\rho}_{\phi\,k^+} + \widehat{\rho}_{\phi\,k^-})$ and $\rho_\theta = \widehat{\rho}_{\theta\,k^+} - \widehat{\rho}_{\theta\,k^-}$.

Note that all linearization parameters (Equation D.15 to Equation D.18) depend on known parameters given by the circle solution (see Section 6.1), which makes it very easy to calculate the track direction.

Hit position dependence:. The track angles can be related to the pre-fit triplet parameters (denoted by superscripts $^{\mathrm{pre}}$ or ^{C}) using the fitted residuals:

$$\begin{aligned}\phi_{k^\pm} \;=\; & \varphi^{\mathrm{pre}}_{k^\pm} \;-\; \vec{\boldsymbol{\delta}}^{\top}\,\vec{\boldsymbol{f}}^{\pm}_{\varphi_k} \\ & \mp\; \frac{1}{2}\left[\nu^{\mathrm{pre}}_{k^\pm} \;+\; \kappa\,\rho^{\mathrm{pre}}_{\phi_{k^\pm}} - \vec{\boldsymbol{\delta}}^{\top}\left(\vec{\boldsymbol{f}}^{\pm}_{\nu_k} + \kappa\,\vec{\boldsymbol{f}}^{\pm}_{\rho_{\phi_k}}\right)\right]\end{aligned} \tag{D.20}$$

$$\begin{aligned}\theta_{k^\pm} \;=\; & \theta^{\mathrm{C}}_{k^\pm} \;-\; \vec{\boldsymbol{\delta}}^{\top}\,\vec{\boldsymbol{f}}^{\pm}_{\theta_k} \\ & +\; \left[\tau^{\mathrm{pre}}_{k^\pm} \;+\; \kappa\,\rho^{\mathrm{pre}}_{\theta_{k^\pm}} - \vec{\boldsymbol{\delta}}^{\top}\left(\vec{\boldsymbol{f}}^{\pm}_{\tau_k} \;+\; \kappa\,\vec{\boldsymbol{f}}^{\pm}_{\rho_{\theta_k}}\right)\right],\end{aligned} \tag{D.21}$$

The vectors $\vec{\boldsymbol{f}}^{\pm}_{X}$ are Jacobians whose elements are defined for each hit by the derivatives:

$$(\vec{\boldsymbol{f}}^{\pm}_{X})_{k'} \;:=\; \frac{\partial\, X_\pm}{\partial\,\vec{\delta}_{k'}} \quad \text{with} \quad X = \{\varphi_k,\, \theta_k,\, \nu_k,\, \tau_k,\, \rho_{\phi_k},\, \rho_{\theta_k}\}. \tag{D.22}$$

D.4.1. Small Bending Approximation

In the small bending limit, i.e. $\Phi_{k\,k+1} \ll 1$, the segment length approaches the chord length. The bending angles can then be approximated by:

$$\Phi_{k^\pm} \;\approx\; \pm\kappa\,||\vec{x}_{k\pm1} - \vec{x}_k||. \tag{D.23}$$

and the track direction at hit k is then given by:

$$\phi_{k^\pm} \;=\; \varphi_{k^\pm} \;-\; \vec{\boldsymbol{\delta}}^{\top}\,\vec{\boldsymbol{f}}^{\pm}_{\varphi_k} \;\mp\; \frac{\kappa}{2}\left(||\vec{x}_{k\pm1} - \vec{x}_k|| - \vec{\boldsymbol{\delta}}^{\top}\right)\vec{\boldsymbol{f}}^{\pm}_{\rho_{\phi_k}}, \tag{D.24}$$

$$\theta_{k^\pm} \;=\; \theta_{k^\pm} \;-\; \vec{\boldsymbol{\delta}}^{\top}\,\vec{\boldsymbol{f}}^{\pm}_{\theta_k}. \tag{D.25}$$

D.5. Track Direction Uncertainties

The track direction uncertainties are derived by propagating both the momentum and spatial hit uncertainties in Equation D.20 and Equation D.21. Note that the azimuthal and polar angle uncertainties are fully correlated due to the requirement of momentum conservation. One obtains:

$$\begin{aligned}\mathrm{Var}[\theta_\pm] \;=\; & \left[\vec{\boldsymbol{f}}^{\pm}_{\theta} + \vec{\boldsymbol{f}}^{\pm}_{\tau} + \kappa\,\vec{\boldsymbol{f}}^{\pm}_{\rho_\theta}\right]^{\top}\,\vec{\boldsymbol{\mathrm{C}}}\mathbf{ov}_{\delta}\left[\vec{\boldsymbol{f}}^{\pm}_{\theta} + \vec{\boldsymbol{f}}^{\pm}_{\tau} + \kappa\,\vec{\boldsymbol{f}}^{\pm}_{\rho_\theta}\right] \\ & - 2\left[\vec{\boldsymbol{f}}^{\pm}_{\theta} + \vec{\boldsymbol{f}}^{\pm}_{\tau} + \kappa\,\vec{\boldsymbol{f}}^{\pm}_{\rho_\theta}\right]^{\top}\,\vec{\boldsymbol{\mathrm{C}}}\mathbf{ov}_{\delta/\kappa}\left[\rho_{\theta_\pm} - \vec{\boldsymbol{\delta}}^{\top}\vec{\boldsymbol{f}}^{\pm}_{\rho_\theta}\right] \\ & + \sigma^2_\kappa\left[\rho_{\theta_\pm} - \vec{\boldsymbol{\delta}}^{\top}\vec{\boldsymbol{f}}^{\pm}_{\rho_\theta}\right]^2,\end{aligned} \tag{D.26}$$

$$\begin{aligned}\mathrm{Var}[\phi_\pm] \;=\; & \left[\vec{\boldsymbol{f}}^{\pm}_{\varphi} \mp \frac{1}{2}\left(\vec{\boldsymbol{f}}^{\pm}_{\nu} + \kappa\,\vec{\boldsymbol{f}}^{\pm}_{\rho_\phi}\right)\right]^{\top}\,\vec{\boldsymbol{\mathrm{C}}}\mathbf{ov}_{\delta}\left[\vec{\boldsymbol{f}}^{\pm}_{\varphi} \mp \left(\vec{\boldsymbol{f}}^{\pm}_{\nu} + \kappa\,\vec{\boldsymbol{f}}^{\pm}_{\rho_\phi}\right)\right] \\ & \pm \left[\vec{\boldsymbol{f}}^{\pm}_{\varphi} \mp \frac{1}{2}\left(\vec{\boldsymbol{f}}^{\pm}_{\nu} + \kappa\,\vec{\boldsymbol{f}}^{\pm}_{\rho_\phi}\right)\right]^{\top}\,\vec{\boldsymbol{\mathrm{C}}}\mathbf{ov}_{\delta/\kappa}\left[\rho_{\phi_\pm} - \vec{\boldsymbol{\delta}}^{\top}\vec{\boldsymbol{f}}^{\pm}_{\rho_\phi}\right] \\ & + \frac{1}{4}\sigma^2_\kappa\left[\rho_{\phi_\pm} - \vec{\boldsymbol{\delta}}^{\top}\vec{\boldsymbol{f}}^{\pm}_{\rho_\phi}\right]^2.\end{aligned} \tag{D.27}$$

The first term in Equation D.26 and Equation D.27 comes from the hit position shifts, the last term from the curvature shifts, and the middle term is a combination of both.

The covariance between azimuthal and polar track angle is given by:

$$\begin{aligned}\mathrm{Cov}[\theta_\pm, \phi_\pm] \;=\; & \left[\vec{f}^{\,\pm}_{\theta} + \vec{f}^{\,\pm}_{\tau} + \kappa\, \vec{f}^{\,\pm}_{\rho_\theta}\right]^\top \vec{\mathbf{C}}\mathbf{ov}_{\delta} \left[\vec{f}^{\,\pm}_{\varphi} \mp \frac{1}{2}\left(\vec{f}^{\,\pm}_{\nu} + \kappa\, \vec{f}^{\,\pm}_{\rho_\phi}\right)\right] \\ & \pm \frac{1}{2}\left[\vec{f}^{\,\pm}_{\theta} + \vec{f}^{\,\pm}_{\tau} + \kappa\, \vec{f}^{\,\pm}_{\rho_\theta}\right]^\top \vec{\mathbf{C}}\mathbf{ov}_{\delta/\kappa} \left(\rho_{\phi_\pm} - \vec{\delta}^{\,\top} \vec{f}^{\,\pm}_{\rho_\phi}\right) \\ & - \left[\vec{f}^{\,\pm}_{\varphi} \mp \frac{1}{2}\left(\vec{f}^{\,\pm}_{\nu} + \kappa\, \vec{f}^{\,\pm}_{\rho_\phi}\right)\right]^\top \vec{\mathbf{C}}\mathbf{ov}_{\delta/\kappa} \left(\rho_{\theta_\pm} - \vec{\delta}^{\,\top} \vec{f}^{\,\pm}_{\rho_\theta}\right) \\ & \mp \frac{1}{2}\,\sigma^2_\kappa \left(\rho_{\theta_\pm} - \vec{\delta}^{\,\top} \vec{f}^{\,\pm}_{\rho_\theta}\right)\left(\rho_{\phi_\pm} - \vec{\delta}^{\,\top} \vec{f}^{\,\pm}_{\rho_\phi}\right). \end{aligned} \tag{D.28}$$

The covariance between the track angles and the curvature is given by:

$$\mathrm{Cov}[\kappa, \theta_\pm] \;=\; \sigma^2_\kappa \left(\rho_{\theta_\pm} - \vec{\delta}^{\,\top} \vec{f}^{\,\pm}_{\rho_\theta}\right) - \left[\vec{f}^{\,\pm}_{\theta} + \vec{f}^{\,\pm}_{\tau} + \kappa\, \vec{f}^{\,\pm}_{\rho_\theta}\right]^\top \vec{\mathbf{C}}\mathbf{ov}_{\delta/\kappa}, \tag{D.29}$$

$$\begin{aligned}\mathrm{Cov}[\kappa, \phi_\pm] \;=\; & \mp \frac{1}{2}\,\sigma^2_\kappa \left(\rho_{\phi_\pm} - \vec{\delta}^{\,\top} \vec{f}^{\,\pm}_{\rho_\phi}\right) \\ & - \left[\vec{f}^{\,\pm}_{\varphi} \mp \frac{1}{2}\left(\vec{f}^{\,\pm}_{\nu} + \kappa\, \vec{f}^{\,\pm}_{\rho_\phi}\right)\right]^\top \vec{\mathbf{C}}\mathbf{ov}_{\delta/\kappa}. \end{aligned} \tag{D.30}$$

Finally, the covariance between the track angles and the track position is given by:

$$\mathrm{Cov}[\vec{\delta}, \theta_\pm] \;=\; -\,\vec{\mathbf{C}}\mathbf{ov}_{\delta} \left[\vec{f}^{\,\pm}_{\theta} + \vec{f}^{\,\pm}_{\tau} + \kappa\, \vec{f}^{\,\pm}_{\rho_\theta}\right] + \vec{\mathbf{C}}\mathbf{ov}_{\delta/\kappa} \left(\rho_{\theta_\pm} - \vec{\delta}^{\,\top} \vec{f}^{\,\pm}_{\rho_\theta}\right), \tag{D.31}$$

$$\begin{aligned}\mathrm{Cov}[\vec{\delta}, \phi_\pm] \;=\; & -\,\vec{\mathbf{C}}\mathbf{ov}_{\delta} \left[\vec{f}^{\,\pm}_{\varphi} \mp \frac{1}{2}\left(\vec{f}^{\,\pm}_{\nu} + \kappa\, \vec{f}^{\,\pm}_{\rho_\phi}\right)\right] \\ & \mp \frac{1}{2}\,\vec{\mathbf{C}}\mathbf{ov}_{\delta/\kappa} \left(\rho_{\phi_\pm} - \vec{\delta}^{\,\top} \vec{f}^{\,\pm}_{\rho_\phi}\right). \end{aligned} \tag{D.32}$$

All formulas above have been validated by a numerical simulation.

E. Gap Spectrometer Dipole

Figure E.11 shows the simplest spectrometer setup with three detector planes (triplet) and one gap dipole. Note that the notation of variables here differs from the case of a uniform magnetic field in the previous section. The gap dipole is placed between detector layers 1 and 2 at distances ν_1 and ν_2, respectively, and has a gap size of ν_B. In the following, it is assumed that all measurement planes and the gap dipole entrance and exit windows are parallel. The magnetic field is pointing in z-direction such that the x-y plane is the bending plane.

The elevation angle, β, measures the particle angle with respect to the x-y plane and is related to the polar angle via $\theta = \pi/2 - \beta$. Note that the elevation angle is an invariant in the plane transverse to the magnetic field, i.e., $\beta_1 = \beta_\mathrm{B} = \beta_2$.

Since the region between tracking layers L0 and L1 has no magnetic field, it is easy to calculate the angles φ_0 and β_0 for the first segment. For the trajectory between tracking layers L1 and L2, the situation is far more complicated: the trajectory has first a field-free segment, then a magnetic field segment, and then another field-free segment.

First, the trajectory in the bending plane is calculated. The bending angle, Φ, is defined as ratio of the arc length, s_B, over the bending radius, R. Both parameters are related to the gap size, ν_B, through:

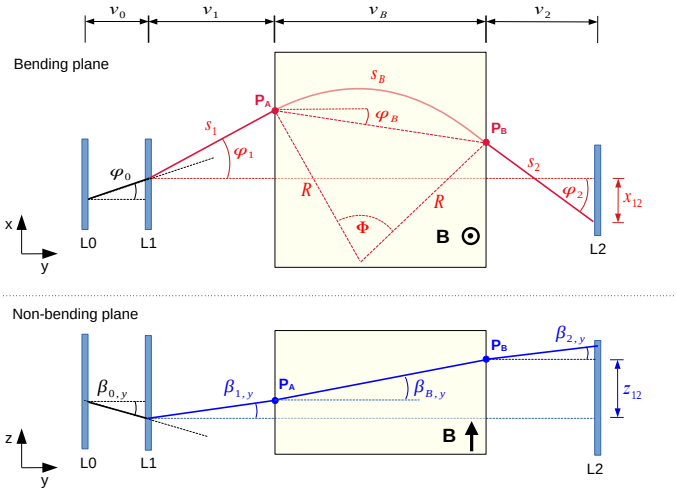

Figure E.11: Sketch of a gap spectrometer dipole with three layers (L0-L2) with L1 being the scattering layer of the triplet. The upper half shows the (x-y) bending plane and the definition of the azimuthal angles for the different track segments and the bending angle Φ; the lower half shows the (y-z) plane with the elevation angles β projected to the y-axis.

$$\Phi = \frac{s_B}{R} \;=\; 2\,\arcsin\frac{\nu_\mathrm{B}}{2R\cos\varphi_\mathrm{B}}, \tag{E.1}$$

with $\cos\varphi_\mathrm{B}$ being the average azimuthal angle in the field region[19]. The azimuthal angles in the field-free region are related to the bending angle in the field via:

$$\varphi_{1,2} = \varphi_\mathrm{B} \mp \frac{\Phi}{2}. \tag{E.2}$$

With the above relation, the bending radius in Equation E.1 is calculated as function of the azimuthal angle φ_1:

$$R = \frac{\nu_\mathrm{B}}{\sin(\varphi_1 + \Phi) - \sin\varphi_1}. \tag{E.3}$$

The horizontal offset, $x_{12} := x_2 - x_1$, measured between tracking layers L1 and L2, is a function of all azimuthal angles:

$$\begin{aligned} x_{12} \;&=\; \nu_1 \tan\varphi_1 + \nu_\mathrm{B} \tan\varphi_\mathrm{B} + \nu_2 \tan\varphi_2 \\ &=\; \nu_1 \tan\varphi_1 + \nu_\mathrm{B} \tan\left(\varphi_1 + \frac{\Phi}{2}\right) + \nu_2 \tan\left(\varphi_1 + \Phi\right). \end{aligned} \tag{E.4}$$

Since ν_1, ν_2 and ν_3 are geometric constants, and x_{12} is a measured quantity, Equation E.4 defines a unique relationship between the azimuthal angle φ_1 and the bending angle Φ. This relation, however, is highly non-linear in both φ_1 and $\Phi/2$, making it difficult to derive a solution

[19] In this calculation, stray fields are neglected.

for the general case (see also Section E.1).

In the non-bending plane, the elevation angle, β_1, is given through the relation:

$$\tan\beta_1 \;=\; \frac{z_{12}}{s_1 + s_B + s_2}, \tag{E.5}$$

with z_{12} being the measured vertical offset, $z_{12} := z_2 - z_1$. The parameters s_1 and s_2 are the lengths of the no-field track segments in the bending plane, given by:

$$s_1 = \nu_1 \sec\varphi_1, \tag{E.6}$$
$$s_2 = \nu_2 \sec(\varphi_1 + \Phi_{\varphi_1}). \tag{E.7}$$

Here the notation $\Phi_{\varphi_1} := \Phi(\varphi_1)$ is used, where the index indicates the functional dependence given by Equation E.4.

Finally, using the bending radius (Equation E.3) and the relation for the elevation angle (Equation E.5) the 3D curvature is calculated as:

$$\kappa = R^{-1}\cos\beta_1 \;=\; \frac{\sin(\varphi_1+\Phi_{\varphi_1}) - \sin\varphi_1}{\nu_\mathrm{B}} \times \frac{1}{\sqrt{1 + \frac{z_{12}^2}{\left(\nu_1\sin\varphi_1 + \nu_2\sin(\varphi_1+\Phi_{\varphi_1}) + \nu_\mathrm{B}\frac{\Phi_{\varphi_1}}{\sin(\varphi_1+\Phi_{\varphi_1})-\sin\varphi_1}\right)^2}}}. \tag{E.8}$$

This equation is non-linear in φ_1 and Φ_{φ_1}. Since the function $\Phi(\varphi_1)$ is also non-linear, the linearization around a reference solution is here much more complicated than in the case of a triplet in a uniform magnetic field (Section 6.1).

As motivated in Section 2, the solution with zero kink angle in the bending plane, $\varphi_{1,\mathrm{ref}} = \varphi_0$, is chosen as reference for the linearization. In the following, the solution for the general case and the small bending approximation is discussed.

E.1. General Solution

The general solution involves solving Equation E.4 numerically to determine the reference bending angle $\Phi_\mathrm{ref} = \Phi(\varphi_{1,\mathrm{ref}})$. With the help of Φ_ref, all parameters of the reference trajectory can be calculated; most importantly, the reference elevation angle β_ref (Equation E.5), and the reference curvature κ_ref (Equation E.8).

For the determination of the ρ parameters, the derivatives $\mathrm{d}\kappa/\,\mathrm{d}\varphi_1$ and $\mathrm{d}\kappa/\,\mathrm{d}\theta_1$ are needed. An analytical solution can be derived by differentiation of Equation E.8 and Equation E.5, respectively, and by using the relations:

$$\rho_\theta \;=\; \rho_\phi \frac{\partial(\Delta\theta)}{\partial(\Delta\phi)} \;=\; \rho_\phi \frac{\partial\theta_1}{\partial\varphi_1} \;=\; -\rho_\phi \frac{\partial\beta_1}{\partial\varphi_1}. \tag{E.9}$$

However, the equations obtained in this way will be very unwieldy. In fact, it is much easier to determine the ρ parameters numerically from a small variation, ϵ, of the azimuthal angle $\varphi_{1,\mathrm{ref}} \to \varphi^\epsilon_{1,\mathrm{ref}} = \varphi_{1,\mathrm{ref}} + \epsilon_\varphi$. This yields a second solution, which is denoted as $\kappa^\epsilon_\mathrm{ref}$ and $\beta^\epsilon_{1,\mathrm{ref}}$. The fundamental triplet parameters are then given by:

$$\rho_\theta = -\frac{\beta^\epsilon_{1,\mathrm{ref}} - \beta_{1,\mathrm{ref}}}{\kappa^\epsilon_\mathrm{ref} - \kappa_\mathrm{ref}}, \tag{E.10}$$
$$\rho_\phi = \frac{\epsilon_\varphi}{\kappa^\epsilon_\mathrm{ref} - \kappa_\mathrm{ref}}, \tag{E.11}$$
$$\tilde\Theta = -\rho_\theta\,\kappa_\mathrm{ref} - (\beta_{1,\mathrm{ref}} - \beta_0), \tag{E.12}$$
$$\tilde\Phi = -\rho_\phi\,\kappa_\mathrm{ref}. \tag{E.13}$$

E.2. Approximation for Small Bending Angles

In the case of small bending angles Φ, Equation E.4 can be linearized to first order in Φ. In this approximation, the fundamental triplet parameters are given by:

$$\tilde\Phi \approx \arctan\left(\frac{x_{12}}{y_{12}}\right) - \varphi_0, \tag{E.14}$$
$$\tilde\Theta \approx \arctan\left(\frac{z_{12}}{d_{12}}\right) - \theta_0, \tag{E.15}$$
$$\rho_\phi \approx -\frac{\sqrt{d_{12}^2 + z_{12}^2}}{2}\,\frac{\nu_B}{y_{12}}\left(1 - \frac{\nu_2 - \nu_1}{y_{12}}\right), \tag{E.16}$$
$$\rho_\theta \approx 0, \tag{E.17}$$

with $d_{12} := \sqrt{x_{12}^2 + y_{12}^2}$ being the distance between hit 1 and 2 in the bending plane. Similar to the weak bending case in a uniform magnetic field, the parameter ρ_θ vanishes here. For symmetric setups, i.e., $\nu_1 = \nu_2$, the parameter ρ_ϕ is equivalent to half the effective track length in the dipole field. In the limit $\nu_1 \to 0$ and $\nu_2 \to 0$ (the tracking layer L1 and L2 are positioned at the dipole entrances and exit), this parameter becomes: $\rho_\phi = -\sqrt{d_{12}^2 + z_{12}^2}/2$. Similar to the uniform magnetic field setup, the ρ_ϕ parameter corresponds to half the length that the particle travels in the magnetic field, consistent with the naive expectation from the Lorentz force law.

F. Triplet with General Field Configuration

An inhomogeneous or irregular magnetic field represents the greatest challenge for the calculation of the triplet parameters. The main difficulty is that trajectories connecting the hit positions $\vec{x}_0$, $\vec{x}_1$, and $\vec{x}_2$ need to be found, and this by means of track extrapolation since no analytical solution exists, see also Figure F.12.

In the following, an algorithm is presented that finds a reference trajectory for an arbitrary (inhomogeneous) magnetic field by means of track extrapolation. This algorithm will be used to calculate the fundamental triplet parameters and the hit gradients.

F.1. Finding a Reference Trajectory

In the following, it is assumed that an approximate solution for the hit triplet exists and is known. This could be, for example, a solution obtained with a constant averaged

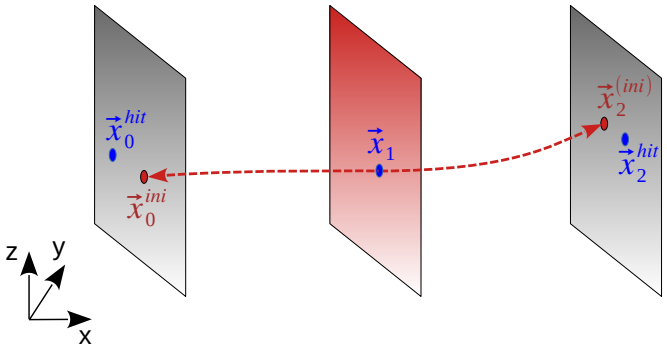

Figure F.12: Sketch showing the first step of the extrapolation algorithm for inhomogeneous magnetic fields. The *red dashed* line shows the trajectory obtained by extrapolating the track vector at the middle layer from the hit position $\vec{x}_1$ to both sides.

magnetic field strength. The reference trajectory can then be found using Newton's method in 2 dimensions ($\theta - \phi$ space). A procedure tailored for hit triplets is described in the following paragraphs.

At the middle hit position, the initial approximated solution is described by five track parameters:

- κ^{ini}: 3D curvature of the approximate trajectory;
- θ_{10}^{ini} (θ_{12}^{ini}): polar angle of the track at the middle hit position before (after) scattering;
- ϕ_{10}^{ini} (ϕ_{12}^{ini}): azimuthal angle of the track at the middle hit position before (after) scattering.

By extrapolating the trajectory from the middle hit position to both sides, as sketched in Figure F.12, the extrapolated hit positions $\vec{x}_0^{\,\text{ini}}$ and $\vec{x}_2(0) = \vec{x}_2^{\,\text{ini}}$ are obtained. In the next step, the polar and azimuthal angles are varied by ϵ_θ and ϵ_ϕ, respectively, and a new set of angles is obtained for track extrapolations:

$$\left.\begin{aligned} \theta_{1k}^{(\epsilon_\theta)} &= \theta_{1k}^{\text{ini}} + \epsilon_\theta \\ \phi_{1k}^{(\epsilon_\phi)} &= \phi_{1k}^{\text{ini}} + \epsilon_\phi \end{aligned}\right\} \quad k = 0, 2 \qquad \text{(F.1)}$$

Two more extrapolations to the tracking planes L0 and L2 are performed on each side. Let $\vec{x}_k^{\,(\epsilon_\theta)}$ and $\vec{x}_k^{\,(\epsilon_\phi)}$ be the extrapolated points from the polar angle and azimuthal angle variations, respectively, the matching condition reads:

$$\vec{x}_k' = \vec{x}_k + \eta_{\theta,k}\,\frac{\vec{x}_k^{\,(\epsilon_\theta)} - \vec{x}_k^{\,\text{ini}}}{\epsilon_\theta} + \eta_{\phi,k}\,\frac{\vec{x}_k^{\,(\epsilon_\phi)} - \vec{x}_k^{\,\text{ini}}}{\epsilon_\phi} \stackrel{!}{=} \vec{x}_k^{\,\text{hit}},$$

with $\vec{x}_k'$ being the calculated interception points and $\vec{x}_k^{\,\text{hit}}$ being the measured hit positions. For each side ($k = 0, 2$), a system of three equations with two unknown correction parameters: $\eta_{\theta,k}$ and $\eta_{\phi,k}$ are obtained. The third degree of freedom corresponds to the segment length, which is indirectly determined by the extrapolation procedure.

Above system of equations can be solved by minimizing the spatial distance $||\vec{x}_k^{\,\text{hit}} - \vec{x}_k'||$. Using the short-hand notations:

$$\begin{aligned} \vec{a}_{\theta,k} &:= \vec{x}_k^{\,(\epsilon_\theta)} - \vec{x}_k^{\,\text{ini}}, \\ \vec{a}_{\phi,k} &:= \vec{x}_k^{\,(\epsilon_\phi)} - \vec{x}_k^{\,\text{ini}}, \end{aligned}$$

the solution for each side ($k = 0, 2$) is given by:

$$\begin{pmatrix} \eta_{\theta,k}/\epsilon_\theta \\ \eta_{\phi,k}/\epsilon_\phi \end{pmatrix} = \frac{\vec{x}_k^{\,\text{hit}} - \vec{x}_k^{\,\text{ini}}}{\vec{a}_{\theta,k}^{\,2}\,\vec{a}_{\phi,k}^{\,2} - (\vec{a}_{\theta,k}\,\vec{a}_{\phi,k})^2} \cdot \begin{pmatrix} \vec{a}_{\phi,k}^{\,2}\,\vec{a}_{\theta,k} - (\vec{a}_{\theta,k}\,\vec{a}_{\phi,k})\,\vec{a}_{\phi,k} \\ \vec{a}_{\theta,k}^{\,2}\,\vec{a}_{\phi,k} - (\vec{a}_{\theta,k}\,\vec{a}_{\phi,k})\,\vec{a}_{\theta,k} \end{pmatrix}. \qquad \text{(F.2)}$$

In case of non-linearities, the matching condition might not be fulfilled in one extrapolation step and the procedure needs to be iterated until $\eta_{\theta,k}$ and $\eta_{\phi,k}$ are determined with the required accuracy, i.e., $||\vec{x}_k' - \vec{x}_k^{\,\text{hit}}|| <$ accuracy. Finally, the track parameters for the reference solution at the middle layer are given by:

$$\theta_{1k} = \theta_{1k}^{\text{ini}} + \eta_{\theta_k}, \qquad \text{(F.3)}$$

$$\phi_{1k} = \phi_{1k}^{\text{ini}} + \eta_{\phi_k}. \qquad \text{(F.4)}$$

F.2. Determination of the Triplet Parameters

For the determination of the ρ parameters, the curvature is varied according to:

$$\kappa^{(\epsilon_\kappa)} = \kappa^{\text{ini}} + \epsilon_\kappa. \qquad \text{(F.5)}$$

Using the so modified curvature, the trajectory is extrapolated again from the middle layer to both sides. Similar to the procedure described in Section F.1, a new set of polar $\theta_{1k}^{(\epsilon_\kappa)}$ and azimuthal $\phi_{1k}^{(\epsilon_\kappa)}$ angles is determined such that both reconstructed track segments match the actual hit positions. The four fundamental triplet parameters are then obtained from:

$$\rho_\theta = \frac{\theta_{12}^{(\epsilon_\kappa)} - \theta_{10}^{(\epsilon_\kappa)} - \theta_{12} + \theta_{10}}{\epsilon_\kappa}, \qquad \text{(F.6)}$$

$$\rho_\phi = \frac{\phi_{12}^{(\epsilon_\kappa)} - \phi_{10}^{(\epsilon_\kappa)} - \phi_{12} + \phi_{10}}{\epsilon_\kappa}, \qquad \text{(F.7)}$$

$$\tilde{\Theta} = -\rho_\theta\,\kappa^{\text{ini}} + \theta_{12} - \theta_{10}, \qquad \text{(F.8)}$$

$$\tilde{\Phi} = -\rho_\phi\,\kappa^{\text{ini}} + \phi_{12} - \phi_{10}. \qquad \text{(F.9)}$$

F.3. Determination of the Hit Gradients

For the determination of the hit gradients (see Section 2.2), no further track extrapolations are required. By solving Equation F.2 for the in total 3×3 1σ hit position shifts, a set of nine polar and azimuthal angle shifts is obtained, which serves as input for the calculation of the hit gradients according to Equation 15 and 16.

To summarize, for the determination of the triplet parameters, at least four track extrapolations are needed for

each segment of the triplet: one for the starting trajectory (estimate), two for the track direction variation, and one for the curvature variation. In case of large non-linearities, more extrapolations might be required. This method is universal and can be used for any tracking detector with any arbitrary field configuration.

References

[1] R. E. Kálmán, A new approach to linear filtering and prediction problems, J. Basic Eng. 82 (1) (1960) 35. doi:10.1115/1.3662552.
URL http://FluidsEngineering.asmedigitalcollection.asme.org/article.aspx?articleid=1430402

[2] R. Frühwirth, Application of Kalman filtering to track and vertex fitting, Nucl. Instrum. Meth. A 262 (1987) 444–450. doi:10.1016/0168-9002(87)90887-4.

[3] V. Blobel, A new fast track-fit algorithm based on broken lines, Nucl. Instrum. Meth. A 566 (2006) 14–17. doi:10.1016/j.nima.2006.05.156.

[4] C. Kleinwort, General Broken Lines as advanced track fitting method, Nucl. Instrum. Meth. A 673 (2012) 107–110. arXiv:1201.4320, doi:10.1016/j.nima.2012.01.024.

[5] V. Blobel, Software alignment for tracking detectors, Nucl. Instrum. Meth. A 566 (2006) 5–13. doi:10.1016/j.nima.2006.05.157.

[6] V. Blobel, C. Kleinwort, F. Meier, Fast alignment of a complex tracking detector using advanced track models, Comput. Phys. Commun. 182 (2011) 1760–1763. arXiv:1103.3909, doi:10.1016/j.cpc.2011.03.017.

[7] N. Berger, A. Kozlinskiy, M. Kiehn, A. Schöning, "A new three-dimensional track fit with multiple scattering", Nucl. Instrum. Methods Phys. Res. A: Accelerators, Spectrometers, Detectors and Associated Equipment **844** (2017) 135 – 140. doi:https://doi.org/10.1016/j.nima.2016.11.012.

[8] T. Kar, A. Schöning, A Triplet Track Trigger for the FCC-hh to improve the measurement of Di-Higgs production and the Higgs self-coupling, Nucl. Instrum. Meth. A 1072 (2025) 170085. arXiv:2401.16046, doi:10.1016/j.nima.2024.170085.

[9] K. Arndt, et al., "Technical design of the phase I Mu3e experiment", Nucl. Instrum. Meth. A 1014 (2021) 165679. arXiv:2009.11690, doi:10.1016/j.nima.2021.165679.

[10] A. Kozlinskiy, Track reconstruction for the Mu3e experiment based on a novel Multiple Scattering fit, EPJ Web Conf. 150 (2017) 00005. doi:10.1051/epjconf/201715000005.

[11] D. vom Bruch, Online Data Reduction using Track and Vertex Reconstruction on GPUs for the Mu3e Experiment, EPJ Web Conf. 150 (2017) 00013. doi:10.1051/epjconf/201715000013.

[12] A. Schöning, A New Track Reconstruction Algorithm suitable for Parallel Processing based on Hit Triplets and Broken Lines, EPJ Web Conf. 127 (2016) 00015. doi:10.1051/epjconf/201612700015.

[13] V. L. Highland, "Some practical remarks on multiple scattering", Nucl. Inst. & Meth. A **129** (1975) 497–499. doi:10.1016/0029-554X(75)90743-0.

[14] G. R. Lynch, O. I. Dahl, Approximations to multiple Coulomb scattering, Nucl. Instrum. Meth. B 58 (1991) 6–10. doi:10.1016/0168-583X(91)95671-Y.

[15] A. A. Alves, Jr., et al., The LHCb Detector at the LHC, JINST 3 (2008) S08005. doi:10.1088/1748-0221/3/08/S08005.

[16] R. Diestel, Graph Theory, Springer, 2017. doi:10.1007/978-3-662-53622-3.

[17] F. Scarselli, et al., The Graph Neural Network Model, IEEE Transactions on Neural Networks 20 (1) (2009) 61–80. doi:10.1109/TNN.2008.2005605.

[18] T. Toffoli, N. H. Margolus, Cellular Automata Machines: A New Environment for Modelling, MIT Press, Cambridge, MA, 1987. doi:10.7551/mitpress/1763.001.0001.

[19] S. Gupta, Track Reconstruction Using Cellular Automata for the High Luminosity LHC (2024).
URL https://www.physi.uni-heidelberg.de/Publications/

[20] D. Colella, ALICE ITS upgrade for LHC Run 3: commissioning in the laboratory, J. Phys. Conf. Ser. 2374 (1) (2022) 012058. arXiv:2106.16168, doi:10.1088/1742-6596/2374/1/012058.

[21] B. Abelev, et al., Technical Design Report for the Upgrade of the ALICE Inner Tracking System, J. Phys. G 41 (2014) 087002. doi:10.1088/0954-3899/41/8/087002.

[22] ATLAS Collaboration, "Technical Design Report for the ATLAS ITk Pixel Detector", Tech. Rep. ATL-COM-ITK-2018-019, CERN, Geneva (Mar 2018).
URL https://cds.cern.ch/record/2310230

[23] G. Aglieri Rinella, The ALPIDE pixel sensor chip for the upgrade of the ALICE Inner Tracking System, Nucl. Instrum. Meth. A 845 (2017) 583–587. doi:10.1016/j.nima.2016.05.016.